Inorganic Chemistry

Article

pubs.acs.org/IC

Electronic Structures of Homoleptic [Tris(2,2′-bipyridine)M]^n Complexes of the Early Transition Metals (M = Sc, Y, Ti, Zr, Hf, V, Nb, Ta; n = 1+, 0, 1−, 2−, 3−): An Experimental and Density Functional Theoretical Study

Amanda C. Bowman,[§] Jason England,[†] Stephen Sproules,[‡] Thomas Weyhermüller,[†] and Karl Wieghardt*[,†]

[†]Max-Planck-Institut für Chemische Energiekonversion, Stiftstrasse 34-36, D-45470 Mülheim an der Ruhr, Germany

[‡]School of Chemistry and Photon Science Institute, The University of Manchester, Oxford Road, Manchester M13 9PL, United Kingdom

Supporting Information

ABSTRACT: The electronic structures of the complexes $[M(^tbpy)_3]^{0,1-}$ (M = Nb, Ta; ^{t}bpy = 4,4′-di-*tert*-butyl-2,2′-bipyridine) have been investigated using a combination of UV−vis spectroscopy, EPR spectroscopy, and XAS. Furthermore, the crystal structure of $[Na(THF)_5][Ta(^tbpy)_3]$ has been determined. These studies were supplemented by density functional theory (DFT) and the calculations extended to include the series $[Y(bpy)_3]^m$ (m = 0, 1−, 2−, 3−), $[Ti(bpy)_3]^n$ (n = 1+, 0, 1−, 2−, 3−), $[Zr(bpy)_3]^p$, and $[Hf(bpy)_3]^p$ (p = 0, 1−, 2−). This has allowed us to define the correct electronic structures of these early transition metal tris(2,2′-bipyridine) complexes. It is shown that in the $[Y(bpy)_3]^m$ series the central ion possesses an invariant +III oxidation state and that the three successive one-electron redox processes that comprise the series are solely ligand-based, yielding three $(bpy^{\bullet})^{1-}$ radical anions in the neutral complex through to three diamagnetic dianions $(bpy^{2-})^{2-}$ in the trianion. The same is true for the $[Ti(bpy)_3]^n$ series where the neutral complex contains $3(bpy^{\bullet})^{1-}$ and the trianion $3(bpy^{2-})^{2-}$ anions. Hence, the central ion always possesses a central Ti^{III} (d^1) ion that intramolecularly antiferromagnetically couples to any $(bpy^{\bullet})^{1-}$ ligands present. In contrast, the central metal ions in the series $[Zr(bpy)_3]^p$ and $[Hf(bpy)_3]^p$ always possess a +IV oxidation state; hence, the dianions contain three $(bpy^{2-})^{2-}$ ligands and yield an S = 0 ground state. The electronic structures of the neutral Nb and Ta analogues possessing $S = {}^1/_2$ ground states are best described as $[Nb^{IV}(bpy^{2-})_2(bpy)^0)]^0$ and $[Ta^V(bpy^{\bullet})(bpy^{2-})_2]^0$, and their S = 0 monoanions as $[Nb^{IV}(bpy^{\bullet})(bpy^{2-})_2]^{1-}$ and $[Ta^V(bpy^{2-})_3]^{1-}$. The central metal ion in the Nb series maintains a +IV oxidation state, while in the Ta series the central metal ion displays a +V oxidation state throughout.

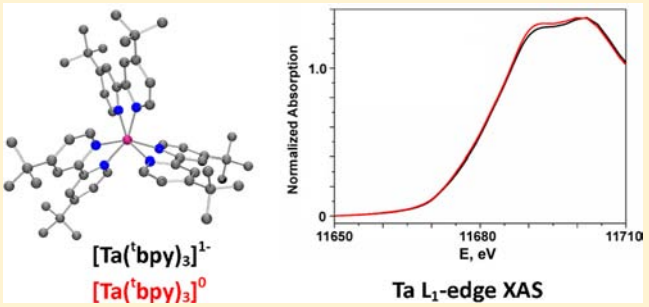

INTRODUCTION

Early transition metal tris(2,2′-bipyridine) complexes (M = Sc, Y, Ti, Zr, Hf, V, Nb, Ta) with charges ranging from 1+ to 3−, accessible via successive one-electron transfer steps, have been generated either chemically or electrochemically, and in many instances isolated as neutral species or salts.[1,2] Table 1 provides a list of the complexes isolated to date and their electronic ground states.[3−17] Despite the fact that many of the complexes shown in Table 1 have been synthesized as early as the mid 1960s, in only a few cases have their electronic structures been elucidated spectroscopically (using UV−vis and EPR, and magnetochemically) and correctly described.

It is now well established that 2,2′-bipyridine is a redox-active (noninnocent) ligand that can be N,N′-coordinated either as a neutral ligand (bpy^0) (S = 0), a π radical anion $(bpy^{\bullet})^{1-}$ ($S = {}^1/_2$), or a diamagnetic dianion $(bpy^{2-})^{2-}$ (see Scheme 1). It has been demonstrated by cryogenic X-ray crystallography (see Table 2 for the few well documented examples) that these three ligand redox states can be identified by their distinctly different $C_{py}-C_{py}$ and C−N bond distances.[18,19] Recently, this was nicely illustrated in the crystal structures of the following three group 3 transition metal complexes: (a) $[La^{III}Cl_2(Tp^{Me2})(bpy^0)]^0$; (b) $[La^{III}(Tp^{Me2})_2(bpy^{\bullet})]^0$; and (c) $[Y^{III}(Tp^{Me2})(bpy^{2-})(THF)_2]^0$, where $(Tp^{Me2})^{1-}$ represents hydrotris(3,5-dimethylpyrazol-1-yl)borate and THF is tetrahydrofuran.[20] The respective $C_{py}-C_{py}$ and two C−N distances of the M(bpy) chelates contained therein are as follows: (a) 1.484(8), 1.358(7), and 1.337(8) Å; (b) 1.45(2), 1.39(2), and 1.38(2) Å; (c) 1.350(4), 1.434(4), and 1.423(4) Å. These data indicate that the neutral, monoanionic, and dianionic forms of the bpy ligand found in complexes a, b, and c, respectively, have distinct

Received: December 20, 2012
Published: February 6, 2013

   dx.doi.org/10.1021/ic302799s | Inorg. Chem. 2013, 52, 2242−2256

Table 1. Isolated Early Transition Metal Tris(2,2′-bipyridine) Complexes[1,2]

complex	ground state	color	ref
$[Sc(bpy)_3](SCN)_3$	0	colorless	3
$[Sc(bpy)_3]^0$	$^1/_2$	black	4
$[Y(bpy)_3]^0 \cdot 3THF$	$^1/_2$	black	5
$Na_3[Y(bpy)_3] \cdot 6THF$	0	black	6
$[Ti(bpy)_3](BF_4)$	$^1/_2$	violet	7
$[Ti(bpy)_3]^0$	0	violet	8
$Li[Ti(bpy)_3] \cdot 3.7THF$	$^1/_2$	blue-violet	8a, e, 9
$Li_2[Ti(bpy)_3] \cdot 5.7THF$	0		8c, 10
$Na_3[Ti(bpy)_3] \cdot 7THF$	$^1/_2$	black	11
$[Zr(bpy)_3]^0$	0	copper-colored	12, 13
$Li[Zr(bpy)_3]$	$^1/_2$		14
$Li_2[Zr(bpy)_3] \cdot 5THF$	0		14, 15
$[Hf(bpy)_3]^0$	0		13
$[Nb(bpy)_3]^0$	$^1/_2$	violet	16
$[Nb(^tbpy)_3]^0$	$^1/_2$	purple	this work
$Li[Nb(bpy)_3] \cdot 3.5THF$	0	red-violet black	17
$[Ta(bpy)_3]^0$	$^1/_2$		13
$[Ta(^tbpy)_3]^0$	$^1/_2$	purple	this work
$[Na(THF)_5][Ta(^tbpy)_3]$	0	brown black	this work

Scheme 1. Oxidation States of the Bipyridine Ligand, Plus Averaged Crystallographically Determined Bond Distances[a]

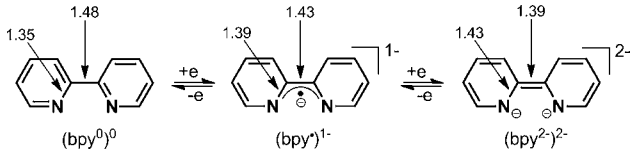

[a]Distances in Å, with error ~ ±0.01 Å. Note: these intrachelate bonds are the focus of all subsequent ligand structure discussions.

$C_{py}-C_{py}$ and C−N distances resulting from the stepwise filling of the LUMO of (bpy^0). Note that the oxidation state of the La and Y ions in these complexes is invariably +III (d^0).

Herein we report the correct electronic structures of so-called "low-valent" $[M(bpy)_3]^n$ complexes of the early transition metals of the first, second, and third rows (i.e., Sc, Y, Ti, Zr, Hf, V, Nb, Ta) that we established, in part, experimentally and (for all complexes) by density functional theory (DFT) calculations. Similar reports have recently been published by us for the series $[Cr(bpy)_3]^n$ (n = 3+, 2+, 1+, 0, 1−, 2−, 3−),[21a] $[V(bpy)_3]^n$ (n = 3+, 2+, 0, 1−),[21b] $[Fe(bpy)_3]^n$ (n = 3+, 2+, 1+, 0, 1−),[21c] and $[Ru(bpy)_3]^n$ (n = 3+, 2+, 1+, 0, 1−).[21c]

EXPERIMENTAL SECTION

Synthesis of Compounds. All reactions were carried out under a purified (water and dioxygen free) argon atmosphere using standard Schlenk techniques, or in a MBraun glovebox. Solvents were dried and deoxygenated according to literature procedures. $NbCl_5$, $TaCl_5$, Hg, Na, and sodium amalgam beads were purchased from Sigma Aldrich and used as received. Tropylium tetrafluoroborate, ferrocenium tetrafluoroborate, and ^{t}bpy (^{t}bpy = 4,4′-di-*tert*-butyl-2,2′-bipyridine) were also purchased from Sigma Aldrich, but were dried *in vacuo* prior to use.

$[Na(THF)_5][Ta(^tbpy)_3]$. To a 250 mL round-bottom flask was added 0.480 g (20.8 mmol) of Na, 48.0 g (239 mmol) of Hg, and approximately 125 mL of THF. The resultant mixture was stirred for 30 min to yield sodium amalgam, to which 1.20 g (3.35 mmol) of $TaCl_5$ and 2.80 g (10.4 mmol) of ^{t}bpy were added. A deep purple color rapidly evolved, but after a further 36 h of stirring the color had changed to dark brown. Subsequently, the reaction mixture was filtered through Celite, the Celite was washed with THF, and all volatiles were removed from the filtrate to give a dark brown powder. The powder was recrystallized from 2:1 THF/diethyl ether at −35 °C to yield 3.10 g (68%) of a dark brown powder identified as $[Na(THF)_5][Ta(^tbpy)_3]$. Anal. Calcd for $C_{74}H_{112}N_6NaO_5Ta$: C, 64.89; H, 8.24; N 6.14. Found: C, 64.56; H, 8.11; N 6.03.

$[Ta(^tbpy)_3]^0$. To a 100 mL round-bottom flask containing 0.340 g (0.248 mmol) of $Na[Ta(^tbpy)_3] \cdot 5THF$ was added approximately 50 mL of THF, and a magnetic stirring bar. In small portions, 0.0438 g (0.246 mmol) tropylium tetrafluoroborate was added with vigorous stirring. Addition of the latter was accompanied by a gradual color change from dark brown to deep purple. After stirring for three hours, all volatiles were removed to give a dark purple powder. The powder was washed with hexanes, and recrystallized from THF at −35 °C to yield 0.225 g (92%) of a dark purple powder identified as $[Ta(^tbpy)_3]^0$. Anal. Calcd for $C_{54}H_{72}N_6Ta$: C, 65.77; H, 7.36; N 8.52. Found: C, 65.98; H, 7.50; N 8.36.

$[Nb(^tbpy)_3]^0$. A mixture of $NbCl_5$ (0.750 g, 2.78 mmol), ^{t}bpy (2.23 g, 8.32 mmol), 6.76 g of sodium amalgam (5 wt %), and 50 mL THF were stirred together for 36 h, over which time a deep indigo color gradually developed. The resultant solution was filtered through Celite, and all volatiles were removed from the filtrate in vacuo to give a dark purple powder. Recrystallization of the purple powder from 2:1 THF/diethyl ether at −35 °C provided 1.62 g (65%) of a dark purple powder identified as $[Nb(^tbpy)_3]^0$. Anal. Calcd for $C_{54}H_{72}N_6Nb$: C, 72.22; H, 8.08; N 9.36. Found: C, 72.48; H, 8.21; N 9.19.

Physical Measurements. Electronic absorption spectra were recorded using a Perkin-Elmer Lambda 19 double-beam spectrophotometer (300−2200 nm). Variable temperature (2−290 K) magnetization data were recorded in a 1 T magnetic field using a MPMS

Table 2. Averaged Experimental C−C and C−N Bond Lengths (Å) of *N,N′*-Coordinated (bpy) Ligands in Selected Crystallographically Characterized Complexes (See the Bond Labeling Diagram)

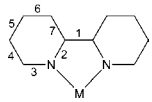

	bond number						
complex	1	2	3	4	5	6	7
$[Al^{III}Cl_2(bpy^0)_2]Cl$[18]	1.48	1.36	1.36	1.39	1.38	1.38	1.38
$Li[Al^{III}(bpy^{2-})_2] \cdot 4THF$[7]	1.36	1.44	1.38	1.35	1.44	1.34	1.42
$[K(2,2,2\text{-crypt})][Fe^{II}(bpy^{\bullet})(mes)]$[19,a]	1.42	1.39	1.35	1.37	1.40	1.35	1.42
$[Li(THF)_4]_2[Zr^{IV}(bpy^{2-})_3]$[15]	1.36	1.44	1.37	1.36	1.43	1.345	1.43
$[Li(THF)_4][Ta^{V}(^tbpy^{2-})_3]$[b]	1.40	1.42	1.40	1.36	1.45	1.36	1.43

[a]2,2,2-crypt = 4,7,13,16,21,24-hexaoxa-1,10-diazabicyclo[8.8.8]hexacosane. [b]This work.

dx.doi.org/10.1021/ic302799s | Inorg. Chem. 2013, 52, 2242−2256

Quantum Design SQUID magnetometer and glass sample holders specifically designed for measurement of air sensitive samples. The experimental magnetic susceptibility data were corrected for underlying diamagnetism using tabulated Pascal's constants. ^{1}H NMR spectra were recorded on a Varian Mercury 400 MHz instrument at ambient temperature. X-band continuous wave EPR spectra measurements were performed using a Bruker E500 ELEXSYS spectrometer and simulated with the XSophe (Bruker Biospin GmbH) suite.[22]

X-ray Absorption Spectroscopy. XAS data were measured at the Stanford Synchrotron Radiation Lightsource (SSRL) with the SPEAR storage ring containing 300 mA at 3.0 GeV. Tantalum L_1-edge spectra were collected on beamline 7-3 operating with a wiggler field of 2 T. A Si(220) double-crystal monochromator was used. Beamline 7-3 is equipped with a rhodium-coated vertical collimating mirror upstream of the monochromator, and a downstream bent-cylindrical focusing mirror (also rhodium-coated). Harmonic rejection was accomplished by detuning the intensity of the incident radiation at the end of the scan by 50%. Incident and transmitted X-ray intensities were monitored using nitrogen-filled ionization chambers. Data were measured in transmittance mode and samples maintained at 10 K using an Oxford Instruments CF1208 continuous flow liquid helium cryostat. For each sample, 6 scans were accumulated, and the energy was calibrated by reference to the absorption of tantalum powder pressed between 38 μm Kapton tape measured simultaneously with each scan, assuming a lowest energy inflection point of 11 682 eV. Data were processed by fitting a second-order polynomial to the pre-edge region and subtracting this background from the entire spectrum.[23] A three-region cubic spline was used to model the smooth background above the edge. The data were normalized by subtracting the spline and normalizing the post-edge to 1.0.

Calculations. All DFT calculations were performed using the ORCA software package.[24] The geometries of all complexes were optimized, in redundant internal coordinates without imposing geometry constraints, and all subsequent single point calculations were performed at the B3LYP level of theory.[25] In all calculations, the def2-TZVP basis set was applied to the metal ions and nitrogen atoms.[26] Whereas the remaining atoms were described for the second and third row transition metal complexes by the slightly smaller polarized split-valence def2-SV(P) basis sets,[27] in the case of the first row transition metal complexes the def2-TZVP basis set minus f polarization functions was used. For compounds including second and third row transition metal ions (Y, Zr, Hf, Nb, Ta), the zeroth-order regular approximation (ZORA) method was implemented.[28] In these calculations ZORA-TZVP and ZORA-SV(P) replaced the standard basis sets TZVP and SV(P), respectively.[28d] Auxiliary basis sets, used to expand the electron density in the calculations, were chosen to match the orbital basis sets.[29] The RIJONX and RIJCOSX approximations were used to accelerate the calculations in the case of the third row transition metal complexes and all others, respectively.[30] In addition to gas phase calculations, all calculations were repeated using the Conductor-like Screening Model (COSMO),[31] with water as the solvent. This caused some reorganization of charge and concomitant minor structural changes in all cases, but did not alter the conclusions of this study, and it is only described in the text where significant. Similarly, the influence of dispersion forces upon the outcome of calculations was probed by implementation of the vdw06 semiempirical correction.[32] This was only found to perturb the outcome of geometry optimization for Ta, and the results detailed for $[Ta(bpy)_3]^n$ and $[Ta(^tbpy)_3]^n$ herein incorporate this van der Waals correction. Additionally, use of vdw06 in single point energy calculations for $[Ti(bpy)_3]^0$ was found to influence the relative ordering of the various calculated electronic states (see below).

The self-consistent field calculations were tightly converged (1×10^{-8} E_h in energy, 1×10^{-7} E_h in the density charge, and 1×10^{-7} in the maximum element of the DIIS[33] error vector). In all cases, the geometries were considered converged after the energy change was less than 1×10^{-6} E_h, the gradient norm and maximum gradient element were smaller than 3×10^{-5} and 1×10^{-4} E_h Bohr^{-1}, respectively, and the root mean displacements of all atoms were smaller than 6×10^{-4} and 1×10^{-3} Bohr, respectively.

Throughout this study, our computational results are described using the broken symmetry (BS) approach.[34] The following notation is used to describe the BS solutions, where the given system is divided into two fragments. The notation BS(m,n) refers to a BS state with m unpaired α-spin electrons localized on fragment 1 and n unpaired β-spin electrons localized on fragment 2. In most cases, fragments 1 and 2 correspond to the metal and the ligands, respectively. In this notation the standard high-spin, open-shell solution is written as BS(m+n,0). The BS(m,n) notation refers to the initial guess for the wave function. The variational process does, however, have the freedom to converge to a solution of the form BS(m−n,0), in which the $n\beta$-spin electrons effectively pair up with $n < m$ α-spin electrons on the partner fragment. Such a solution is then a standard $M_s \cong (m - n)/2$ spin-unrestricted Kohn−Sham solution. As explained elsewhere,[35] the nature of the solution is investigated from the corresponding orbital transformation (COT), which from the corresponding orbital overlaps displays whether the system should be described as a spin-coupled or a closed-shell solution. Orbitals and density plots were created using Chimera.[36]

X-ray Crystallographic Data Collection and Structure Refinement. A black single crystal of $[Na(THF)_5][Ta(^tbpy)_3]$ was coated with perfluoropolyether, picked up with a nylon loop, and immediately mounted in the nitrogen cold stream of the diffractometer to prevent loss of solvent. Graphite monochromated Mo Kα radiation (λ = 0.710 73 Å) from a Mo-target rotating-anode X-ray source was used throughout. Final cell constants were obtained from least-squares fits of several thousand strong reflections. Intensity data were corrected for absorption using intensities of redundant reflections with the program SADABS.[37a] The structure was readily solved by Patterson methods and subsequent difference Fourier techniques. The Siemens ShelXTL[37b] software package was used for solution of and artwork creation for the structures. ShelXL97[37c] was used for the refinement. All non-hydrogen atoms were anisotropically refined, and hydrogen atoms were placed at calculated positions and refined as riding atoms with isotropic displacement parameters. Crystallographic data of the compounds are listed in Table 3.

A split atom model was refined to account for disorder of two out of five THF molecules bound to the sodium cation. A total of 100

Table 3. Crystallographic Data for $[Na(THF)_5][Ta(^tbpy)_3]$

chem formula	$C_{74}H_{112}N_6NaO_5Ta$
fw	1369.64
space group	$P\bar{1}$, No. 2
a, Å	13.775(1)
b, Å	14.105(2)
c, Å	21.909(4)
α, deg	101.8(1)
β, deg	98.28(1)
γ, deg	115.56(1)
V, Å^3	3626.7(9)
Z	2
T, K	100(2)
ρ calcd, g cm^{-3}	1.254
reflns collected/$2\Theta_{max}$	57 688/65.00
unique reflns/$I > 2\sigma(I)$	25 624/21 855
no of params/restraints	834/100
λ, Å /μ(Kα), cm^{-1}	0.710 73/15.73
R1[a]/GOF[b]	0.0651/1.044
wR2[c] ($I > 2\sigma(I)$)	0.1618
residual density, e Å^{-3}	+5.03/−6.38

[a]Observation criterion: $I > 2\sigma(I)$. R1 = $\Sigma||F_o| - |F_c||/\Sigma|F_o|$. [b]GOF = $[\Sigma[w(F_o^2 - F_c^2)^2]/(n - p)]^{1/2}$. [c]wR2 = $[\Sigma[w(F_o^2 - F_c^2)^2]/\Sigma[w(F_o^2)^2]]^{1/2}$ where $w = 1/\sigma^2(F_o^2) + (aP)^2 + bP$, $P = (F_o^2 + 2F_c^2)/3$.

dx.doi.org/10.1021/ic302799s | Inorg. Chem. 2013, 52, 2242−2256

restraints were used to fix bond distances and angles using the SADI instructions of ShelXL97. Thermal displacement parameters of disordered atoms were restrained with EADP.[33]

RESULTS

Syntheses and Spectroscopic Characterization of Complexes. The complexes $[Nb(^tbpy)_3]^0$ and $[Na(THF)_5][Ta(^tbpy)_3]$ have been prepared by reaction of the corresponding pentachlorides MCl_5 (M = Nb, Ta) with 3 equiv of 4,4-di-*tert*-butyl-2,2′-bipyridine and a slight excess of sodium amalgam in water- and oxygen-free THF.[13] Crystalline samples of $[Na(THF)_5][Ta(^tbpy)_3]$ and $[Nb(^tbpy)_3]^0$ were obtained cleanly and in good yields. Oxidation of the monoanion $[Ta(^tbpy)_3]^{1-}$ by 1 equiv of tropylium tetrafluoroborate in THF yields the clean, neutral complex $[Ta(^tbpy)_3]^0$ in very good yields. It has not been possible to isolate the corresponding salt of the anionic species $[Nb(^tbpy)_3]^{1-}$, but the unsubstituted $[Nb(bpy)_3]^{1-}$ complex is already known.[17]

The electronic spectra of the neutral complexes $[M(^tbpy)_3]^0$ (M = V,[21b] Nb, Ta) are presented in Figure 1 and summarized in Table 4 alongside data for $[Ti^{III}(bpy^\bullet)_3]^0$ and $[Cr(^tbpy^\bullet)_3]^0$.

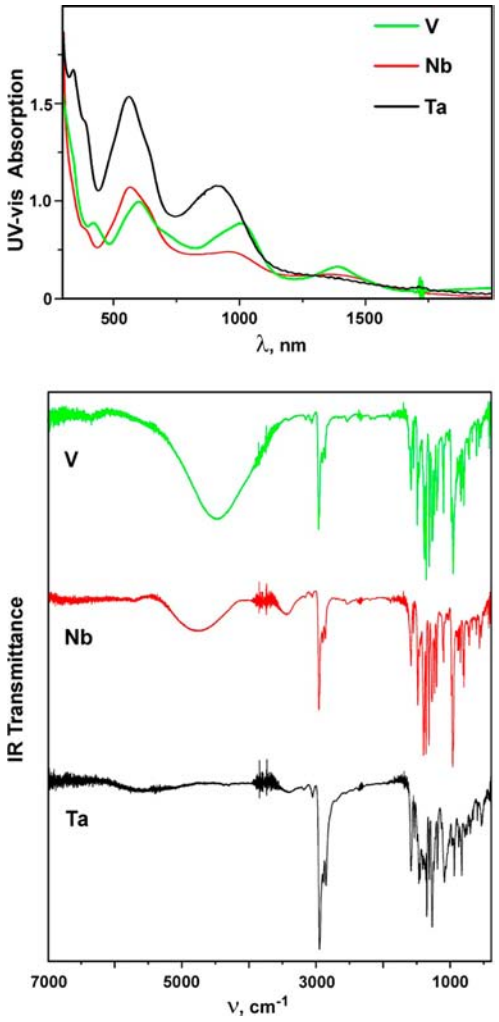

Figure 1. Electronic spectra of the neutral complexes $[M(^tbpy)_3]^0$, where M = V (green line), Nb (red line), and Ta (black line), measured in THF solution at ambient temperature (upper panel). The LLIVCT bands (lower panel) were recorded by IR spectroscopy using KBr disk solid samples.

As has been previously pointed out for $[Cr(^tbpy^\bullet)_3]^0$, all of the aforementioned spectra display a strong similarity to those of the alkali salts of the radical anion $(bpy^\bullet)^{1-}$ and dianion $(bpy^{2-})^{2-}$. The former contain chromophores centered at ~9090, 12 260, and 19 250 cm^{-1}, whereas in the latter $(bpy)^{2-}$ case only two, very intense, bands at ~16 400 and 26 000 cm^{-1} are observed.[38] These absorptions show pronounced vibronic structure and in all cases have been assigned to intraligand $\pi-\pi^*$ transitions. One can assume that the electronic transitions of the complexes in Table 4 have a similar origin. Sadly, due to the overlap of the chromophores associated with the $(bpy^\bullet)^{1-}$ and $(bpy^{2-})^{2-}$, it is not possible to determine the number of each coordinated in the $[M(bpy)_3]^0$ complexes by their electronic spectra alone.

Additionally, the neutral complexes of V, Nb, and Ta display a broad low-energy feature at 4000−5000 cm^{-1} (Table 4), though it is weak in the latter case, that can be assigned as a ligand-to-ligand intervalence charge transfer (LLIVCT) band[39] arising from transition between the ligand-based SOMO of a radical $(bpy^\bullet)^{1-}$ and an empty ligand-based LUMO of (bpy^0). This band is absent in the neutral Ti and Cr complexes, which is not surprising because they contain three $(bpy^\bullet)^{1-}$ ligands and a prerequisite for LLIVCT is that the complexes display ligand mixed-valency (i.e., contain at least one $(bpy^\bullet)^{1-}$ and one (bpy^0), or at least one $(bpy^{2-})^{2-}$ and one $(bpy^\bullet)^{1-}$ ligand). For the species $[V^{II}(^tbpy^\bullet)_2(^tbpy^0)]^0$ this assignment has been corroborated by time-dependent (TD)-DFT calculations.[21b]

EPR measurements demonstrate that both $[Nb(^tbpy)_3]^0$ and $[Ta(^tbpy)_3]^0$ display $S = {}^1/_2$ ground states. The corresponding unsubstituted species $[M(bpy)_3]^0$ (M = Nb, Ta) also possess an $S = {}^1/_2$ ground state.[13] In contrast, both $[Na(THF)_5][Ta(^tbpy)_3]$ and $Li[Nb(bpy)_3]\cdot 3.5THF$[17] are diamagnetic. Whereas the EPR spectrum of $[Nb(^tbpy)_3]^0$ was recorded in THF solution at ambient temperature (Figure 2a), that of $[Ta(^tbpy)_3]^0$ was recorded as a powdered solid sample at 20 K (Figure 2b). The latter spectrum displays a narrow (~100 G) signal without any detectable hyperfine splitting from the ^{181}Ta ($I = {}^7/_2$, ~100% natural abundance) isotope. The spectrum is clearly dominated by exchange narrowing where the high sample concentration sees the electron spins exchanging at such a speed so as to reduce the hyperfine field to nearly zero.[40] However, the total magnetic moment of the system is unaffected by electron spin exchange, thereby rendering the *g*-value essentially invariant to exchange narrowing. The spectrum was simulated with $g = 2.011$ and considered indicative of a ligand-based radical rather than a Ta-based unpaired spin, which would ideally show $g < 2$ by virtue of the large spin−orbit coupling constant of the third row metal.

Simulation of the fluid solution EPR spectrum of $[Nb(^tbpy)_3]^0$ (Figure 2a) yielded the parameters $g_{iso} = 1.985$ and $A_{iso}\{^{93}Nb\} = 83 \times 10^{-4}$ cm^{-1} (88.3 G). The 10-line pattern of this spectrum, resulting from a large ^{93}Nb ($I = {}^9/_2$, 100% natural abundance) hyperfine interaction, displays an overall appearance typical of a metal-based spin and reminiscent of the isotropic spectrum of $[V^{II}(^tbpy^\bullet)_2(^tbpy^0)]^0$ and related vanadium tris(dioxolene) and tris(dithiolene) species.[21b,41] Furthermore, the magnitude of the hyperfine coupling is consistent with the large computed Nb content (81%) of the a_1 singly occupied molecular orbital (SOMO) in this D_3 symmetric molecule. In contrast, a considerably larger ^{93}Nb hyperfine coupling of 165 G was measured in the fluid solution spectrum of five-coordinate $K_2[Nb^{IV}O(Pc)]\cdot 5DME$, where $(Pc)^{4-}$ represents the tetraanion of phthalocyanine, with a d_{xy}

dx.doi.org/10.1021/ic302799s | Inorg. Chem. 2013, 52, 2242−2256

Table 4. Electronic Spectra of $[M(^tbpy)_3]^0$ Complexes (M = Ti, V, Cr, Nb, Ta) in Acetonitrile or THF Solution

M[a]	LLIVCT[g]	λ_{max}, cm^{-1} (10^4 ε_{max}, M^{-1} cm^{-1})
Ti[b]		6000 (0.65), 9170 (0.86), 10 700 (0.85), 16 950 (1.35), 2300 (0.67), 12 200 (0.90), 14 400 (1.32)
V[c]	4460	7194 (0.18), 9940(0.39), 16 639(0.50), 23 750 (0.39), 26 670sh (−0.7) 9100sh
Cr[d]		7752 (0.6), 9091 (0.58), 13 333 (0.56), 16 950 (1.05), 19 608 (1.4), 2040 (1.42), 16 390h
Nb[e]	4800	7143 (0.15), 10 204 (0.23), 15 390sh, 17 240 (0.58), 25 000 (0.47)
Ta[f]	5500	7200sh (0.12), 11 111 (0.58), 15 390sh (0.75), 17 240 (0.90), 25 000 (0.85), 26 660 (1.2)

[a]M = Ti, V, Cr taken from ref 8b, and M = Nb, Ta taken from this work. [b]$[Ti^{III}(bpy^{\bullet})_3]^0$ in THF. [c]$[V^{II}(^tbpy^{\bullet})_2(^tbpy^0)]^0$ in THF. [d]$[Cr^{III}(^tbpy^{\bullet})_3]^0$ in CH_3CN. [e]$[Nb^{IV}(^tbpy^{2-})_2(^tbpy^0)]^0$ in THF. [f]$[Ta^{V}(^tbpy^{2-})_2(^tbpy^{\bullet})]^0$ in THF. [g]The transition in this column corresponds to a LLIVCT band observed in the NIR spectrum of a KBr pellet.

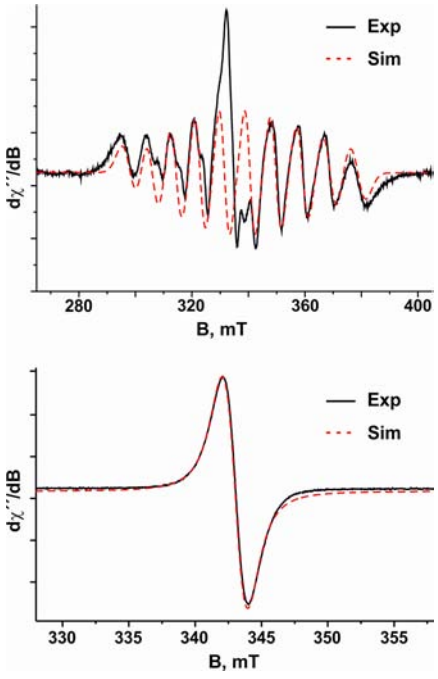

Figure 2. Upper panel: X-band EPR spectrum (black line) and simulation (dashed red line) of $[Nb(^tbpy)_3]^0$ measured in THF solution solution at room temperature (experimental conditions: frequency, 9.4204 GHz; power, 3.16 mW; modulation amplitude, 2.0 mT). Lower panel: X-band EPR spectrum (black line) and simulation (dashed red line) of solid $[Ta(^tbpy)_3]^0$ measured at 20 K (experimental conditions: frequency, 9.6579 GHz; power, 0.06 mW; modulation amplitude, 0.1 mT).

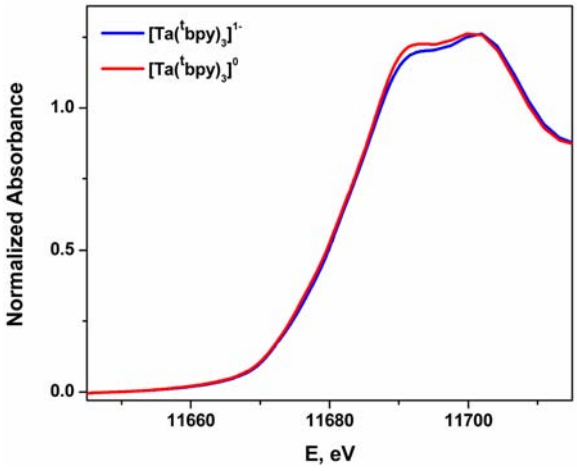

Figure 3. Overlay of the Ta L_1-edge XAS spectra for $[Ta(^tbpy)_3]^0$ (red) and $[Ta(^tbpy)_3]^-$ (blue).

(b_2) SOMO.[42] The spectrum of $[Nb(^tbpy)_3]^0$ shown in Figure 2a also contains a second EPR-active species (≤10%) of unknown origin, most likely corresponding to "free" $(bpy^{\bullet})^{1-}$.

Hence, we can conclude that the electronic structures of neutral $[Nb(^tbpy)_3]^0$ and $[Ta(^tbpy)_3]^0$ are different, despite them sharing a common $S = {}^1/_2$ ground state. Whereas the unpaired electron of the Nb species resides in a metal d-orbital, in the corresponding Ta complex it is predominantly ligand-centered.

Figure 3 shows a comparison of the normalized Ta L_1-edge X-ray absorption spectra of $[Ta(^tbpy)_3]^0$ and $[Na(THF)_5][Ta(^tbpy)_3]$. We have measured at this edge because it is dominated by the Ta 2s → 6p dipole allowed transition and gives roughly the same information as the K-edge as it measures the density of projected p states. Also, the pre-edge is sensitive to local geometry where dipole-forbidden 2s → 5d transitions gain intensity through 5d/6p mixing that is maximized in systems without an inversion center;[43] however, the short core-hole lifetime leads to a substantial line broadening that obscures pre-edge features in these high energy edge measurements. Experimentally, the Ta L_1-edges of the neutral and monoanionic species are superimposable, and they have nearly the same energy 11682.0 and 11682.2 eV, respectively. This reinforces the notion that the tantalum ions have the same oxidation state, namely +V. This contrasts with our recent report that the Re L_1-edge energies of $[Re(bdt)_3]^{2-}$ and $[Re(bdt)_3]^{1-}$ (bdt^{2-} represents benzene-1,2-dithiolate) differ by 1 eV indicating that whereas the former contains a Re^{IV} and $3(bdt)^{2-}$ ligands, the latter contains a Re^{V} ion and $3(bdt)^{2-}$ ligands.[44]

Crystal Structure of $[Na(THF)_5][Ta(^tbpy)_3]$. The crystal structure of $[Na(THF)_5][Ta(^tbpy)_3]$ has been determined by single crystal X-ray crystallography at 100 K using Mo Kα radiation. The structure of the monoanion $[Ta(^tbpy)_3]^{1-}$ is presented in Figure 4, selected bond lengths are summarized in Table 5, and crystallographic details are given in Table 3.

The anion $[Ta(^tbpy)_3]^{1-}$ does not possess any crystallographically imposed symmetry. It is therefore significant that the bond distances and angles of the three *N,N′*-coordinated (bpy) ligands are identical within 3σ limits. The C−C and C−N bond distances in these ligands are very similar to those reported for the diamagnetic dianion $(bpy^{2-})^{2-}$ containing compound $[(bpy^{2-})\{Na^+(dme)\}_2]_\infty$[45] and are significantly different from $[Na(bpy^0)_3]I$,[46] which contains three neutral (bpy^0) ligands. As has been observed in many cases, the C_{py}−C_{py} bond shrinks from 1.48 ± 0.01 Å in neutral (bpy^0) ligands to 1.43 ± 0.01 Å in $(bpy^{\bullet})^{1-}$ radical anions and, finally, to 1.39 ± 0.01 Å in the dianion, which is completely dearomatized (see resonance structure in Scheme 1).[47]

dx.doi.org/10.1021/ic302799s | Inorg. Chem. 2013, 52, 2242−2256

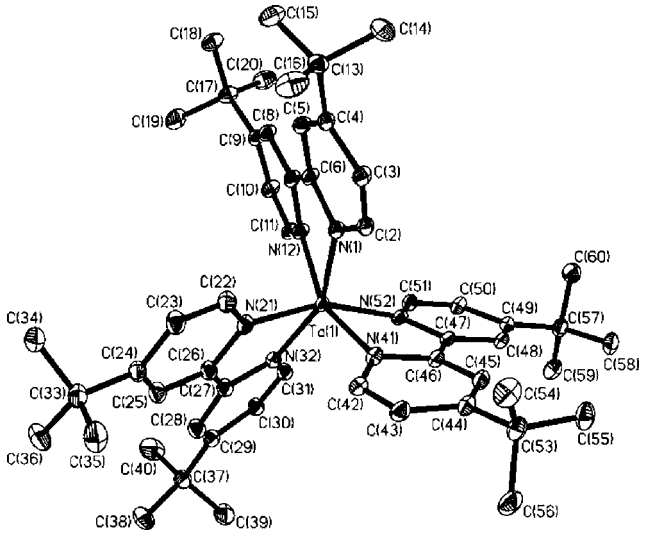

Figure 4. Structure of the monoanion in crystals of $[Na(THF)_5][Ta(^tbpy)_3]$ depicted with 50% probability thermal ellipsoids. Hydrogen atoms and countercation have been omitted for clarity.

Table 5. Selected Experimental Bond Lengths (Å) in the Monoanion $[Ta(^tbpy)_3]^{1-}$

Ta(1)–N(1)		2.083(3)	
Ta(1)–N(12)		2.162(3)	
Ta(1)–N(21)		2.095(4)	
Ta(1)–N(32)		2.159(3)	
Ta(1)–N(41)		2.086(3)	
Ta(1)–N(52)		2.150(3)	
	^{t}bpy 1	^{t}bpy 2	^{t}bpy 3
C(6)–C(7)	1.396(5)	1.394(5)	1.395(5)
N(1)–C(2)	1.404(4)	1.399(5)	1.398(5)
C(2)–C(3)	1.354(5)	1.361(6)	1.349(5)
C(3)–C(4)	1.450(5)	1.448(6)	1.445(6)
C(4)–C(5)	1.360(5)	1.364(6)	1.362(6)
C(5)–C(6)	1.433(5)	1.416(6)	1.434(5)
N(1)–C(6)	1.416(5)	1.422(5)	1.424(5)
C(7)–C(8)	1.431(5)	1.423(5)	1.423(5)
C(8)–C(9)	1.371(5)	1.369(6)	1.363(5)
C(9)–C(10)	1.442(5)	1.441(6)	1.436(5)
C(10)–C(11)	1.360(5)	1.365(5)	1.358(5)
N(12)–C(11)	1.376(5)	1.368(5)	1.379(5)
N(12)–C(7)	1.408(5)	1.411(5)	1.409(5)

A few metal complexes containing *N,N′*-coordinated $(bpy^{2-})^{2-}$ dianions have been characterized by X-ray crystallography, including $[Al^{III}(bpy^{2-})_2]^{1-}$,[48] $[Zr^{IV}(bpy^{2-})_3]^{2-}$,[49] and $[Y^{III}(Tp^{Me2})(bpy^{2-})(THF)_2]^0$.[20] These three all display short C_{py}–C_{py} and long C–N bond distances that are characteristic of the dianion $(^tbpy^{2-})^{2-}$. Similarly, the monoanion $[Ta(^tbpy)_3]^{1-}$ contains three $(^tbpy^{2-})^{2-}$ ligands, and simple arithmetic considerations allow an assignment of the spectroscopic (physical) oxidation state of the central tantalum ion as +V (d^0), yielding the electronic description $[Ta^V(^tbpy^{2-})_3]^{1-}$ ($S = 0$).

Two further aspects of the structure are noteworthy. First, the TaN_6 coordination polyhedron exhibits a twist angle Θ of 32°, which corresponds to a trigonally distorted octahedral geometry. (Whereas the twist angle Θ is 0° in a perfect trigonal prism, the octahedral limit is approximately 45–50° in a tris(bpy) complex due to the relatively acute bite angle associated with bpy coordination.) Second, the two Ta–N bonds of each of the three five-membered $Ta(^tbpy)$ chelate rings are *not* equivalent. Indeed, they differ significantly with one short average Ta–N bond of 2.088(3) Å and a longer one of 2.157(3) Å. It is also interesting that the three protons of each bpy ligand bound to C(2), C(22), and C(42), respectively, are in close contact to the center of a pyridine ring of a neighboring ligand (see Figure 5). Whether this corresponds to repulsive interaction that prevents formation of a more prismatic geometry, or an attractive force that promotes deviation from an octahedral geometry, is not clear at this juncture.

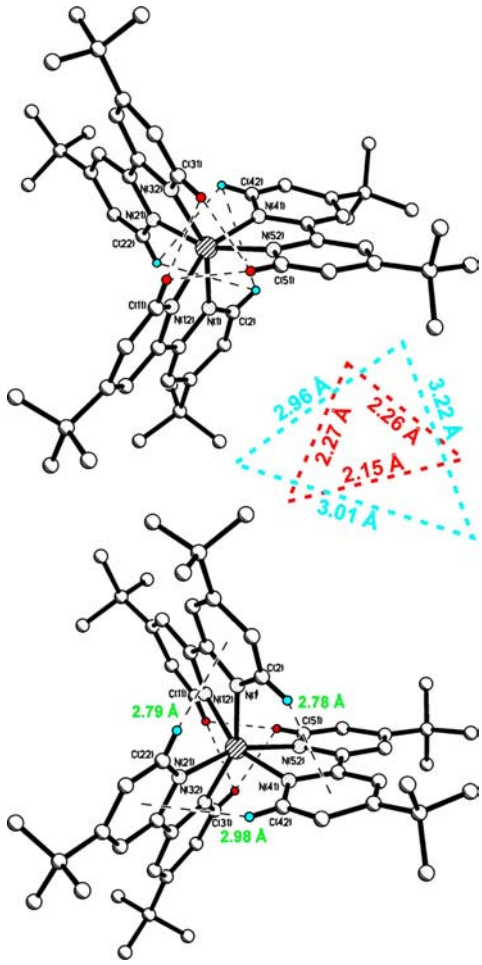

Figure 5. Structure of the monoanion in crystals of $[Na(THF)_5][Ta(^tbpy)_3]$. Top: Emphasizing the shortest intramolecular, nonbonding H···H contacts at 2.15–2.27 Å (red) and 2.96–3.12 Å (blue). Bottom: Shortest distances (2.78–2.98 Å) between the α-pyridyl proton of one ^{t}bpy and the centroid of the pyridyl ring of a neighboring ligand (green). Other hydrogen atoms and the countercation have been omitted for clarity.

DFT Calculations. In order to probe the nature of the electronic and geometric structures of the series of complexes $[M(bpy)_3]^n$, where M = Y, Ti, Zr, Hf, Nb, Ta, we have undertaken a BS DFT study. Calculations of spinn exchange coupling constants, *J*, were performed using the Yamaguchi method, eq 1, where the meaning of the spin expectation values $\langle S^2 \rangle$ and the energies E_{HS} and E_{BS} have been described elsewhere.[34f]

dx.doi.org/10.1021/ic302799s | Inorg. Chem. 2013, 52, 2242–2256

$$J = \frac{E_{HS} - E_{BS}}{\langle S^2\rangle_{HS} - \langle S^2\rangle_{BS}} \quad (1)$$

For all species, geometry optimizations were performed using the B3LYP functional.[25] Subsequent calculation of the ground state electronic structure was undertaken by single point calculations also using the B3LYP functional (see the Experimental Section and Supporting Information for further details). Selected calculated metric parameters are listed in Tables 6 and 7.

Table 6. Average Calculated Bond Distances (Å) for $[Al^{III}(bpy^{\bullet})_3]^0$, $[Al^{III}(bpy^{2-})_3]^{3-}$, and $[Sc^{III}(bpy^{\bullet})_3]^0$ Taken from Reference 21c

complex	method	S	M−N	C−N	C_{py}−C_{py}
$[Al^{III}(bpy^{\bullet})_3]^0$	UKS	$^3/_2{}^b$	2.005, 2.006	1.388, 1.387	1.426
	BS(2,1)	$^1/_2{}^a$	2.004, 2.005	1.388, 1.387	1.426
$[Al^{III}(bpy^{2-})_3]^{3-}$	RKS	0^a	2.045, 2.045	1.434, 1.434	1.392
$[Sc^{III}(bpy^{\bullet})_3]^0$	UKS	$^3/_2{}^b$	2.244, 2.243	1.394, 1.394	1.437
	BS(2,1)	$^1/_2{}^a$	2.241, 2.238	1.392, 1.393	1.438

[a]Ground state. [b]Excited state.

$[Sc^{III}(bpy^{\bullet})_3]^0$ and the $[Y(bpy)_3]^n$ (n = 0, 1−, 2−, 3−) Series. In a previous article we calibrated our computational methodology by calculating the structure of $[Sc(bpy)_3]^0$ ($S = {}^1/_2$),[21c] which is a known complex and for which a magnetic coupling constant J had been experimentally determined (−139 cm^{-1}).[50] Computationally, a central Sc ion with a d^0 configuration and three equivalent $(bpy^{\bullet})^{1-}$ π radical anions that antiferromagnetically couple to one another (J_{calcd} = −162 cm^{-1}) were found, thereby yielding the electronic description $[Sc^{III}(bpy^{\bullet})_3]^0$ ($S = {}^1/_2$ ground state and $S = {}^3/_2$ first excited state). Furthermore, the calculated metrical details of the C−C and C−N bonds (Table 6) closely resemble those found experimentally for uncoordinated $(bpy^{\bullet})^{1-}$. Similar results were also obtained for $[Al^{III}(bpy^{\bullet})_3]^0$ where the experimental J-value[51] of −79 cm^{-1} was well reproduced in a calculated value of −51 cm^{-1}.[21c]

Calculation of $[Y(bpy)_3]^0$ ($S = {}^1/_2$) using unrestricted Kohn−Sham (UKS) and BS(2,1) methodologies converged to the same solution with an electronic structure in which an $S = {}^1/_2$ ground state is attained via an intramolecular antiferromagnetic exchange coupling (J_{calcd} = −108 cm^{-1}) between two $(bpy^{\bullet})^{1-}$ radicals. The remaining "spin-frustrated" unpaired electron resides in a ligand-centered π^* orbital (Figure 6). Thus, the central metal ion is again in its most stable trivalent form (d^0, S = 0), which results in a qualitative MO diagram containing five virtual, empty metal d-orbitals at higher energy (Figure S14). Unsurprisingly, the three equivalent $(bpy^{\bullet})^{1-}$ ligands display C_{py}−C_{py} and C−N distances typical of an uncoordinated $(bpy^{\bullet})^{1-}$ (Table 7), and the structural parameters of the $S = {}^1/_2$ ground and the excited $S = {}^3/_2$ states, each containing three $(bpy^{\bullet})^{1-}$, are identical. Lastly, the geometry of the YN_6 polyhedron is distorted octahedral (Θ = 39°), consistent with the presence of a central d^0 metal ion (Table 7).

A BS(1,1) geometry optimization of the diamagnetic monoanion $[Y(bpy)_3]^{1-}$ (S = 0) revealed the presence of three nearly equivalent reduced bpy ligands. (This solution is ∼4 kcal mol^{-1} lower in energy than the corresponding restricted Kohn−Sham (RKS) solution.) The Mulliken spin population analysis (Figure 6) reveals ∼0 spin on the central metal ion, and 0.9 α- and 2 × 0.47 β-spins on the three bpy ligands (i.e., Y^{III} and $(bpy_3)^{4+}$). Introduction of a strong solvent dielectric during geometry optimization via use of COSMO-(water)[31] localized spins to individual bpy ligands (Figure S13),

Table 7. Calculated Bond Lengths (Å) of *N,N′*-Coordinated Bipyridine Ligands in $[M(bpy)_3]^n$ Complexes

		bpy 1		bpy 2		bpy 3		
complex	Θ^a (deg)	C_{py}−C_{py}	C−N	C_{py}−C_{py}	C−N	C_{py}−C_{py}	C−N	S^b
$[Y^{III}(bpy^{\bullet})_3]^0$	38.7	1.437	1.390, 1.390	1.436	1.390, 1.390	1.436	1.390, 1.390	$^1/_2$
$[Y^{III}(bpy^{2-})(bpy^{\bullet})_2]^{1-}$	38.1	1.434	1.392, 1.392	1.415	1.410, 1.410	1.415	1.410, 1.410	0
$[Y^{III}(bpy^{2-})(bpy^{\bullet})_2]^{1-c}$	38.2	1.436	1.392, 1.392	1.433	1.393, 1.394	1.399	1.431, 1.430	0
$[Y^{III}(bpy^{2-})_2(bpy^{\bullet})]^{2-}$	37.6	1.404	1.422, 1.422	1.407	1.418, 1.418	1.407	1.418, 1.418	$^1/_2$
$[Y^{III}(bpy^{2-})_3]^{3-}$	37.1	1.391	1.437, 1.437	1.390	1.438, 1.437	1.390	1.437, 1.437	0
$[Ti^{III}(bpy^{\bullet})_2(bpy^0)]^{1+}$	48.3	1.449	1.374, 1.370	1.446	1.376, 1.372	1.459	1.365, 1.366	$^1/_2$
$[Ti^{III}(bpy^{\bullet})_3]^0$	46.1	1.432	1.381, 1.382	1.425	1.388, 1.385	1.425	1.385, 1.388	0
$[Ti^{III}(bpy^{\bullet})_2(bpy^{2-})]^{1-}$	45.4	1.410	1.398, 1.398	1.412	1.398, 1.398	1.412	1.397, 1.398	$^1/_2$
$[Ti^{III}(bpy^{\bullet})(bpy^{2-})_2]^{2-}$	42.2	1.399	1.412, 1.412	1.402	1.409, 1.408	1.402	1.408, 1.409	0
$[Ti^{III}(bpy^{2-})_3]^{3-}$	41.4	1.384	1.428, 1.428	1.383	1.429, 1.428	1.383	1.428, 1.429	$^1/_2$
$[Zr^{IV}(bpy^{\bullet})_2(bpy^{2-})]^0$	34.3	1.422	1.399, 1.399	1.427	1.394, 1.394	1.425	1.396, 1.396	0
$[Zr^{IV}(bpy^{\bullet})_2(bpy^{2-})]^{0c}$	41.1	1.435	1.391, 1.391	1.435	1.389, 1.391	1.413	1.411, 1.412	0
$[Zr^{IV}(bpy^{\bullet})(bpy^{2-})_2]^{1-}$	33.3	1.407	1.413, 1.413	1.407	1.413, 1.413	1.408	1.412, 1.413	$^1/_2$
$[Zr^{IV}(bpy^{2-})_3]^{2-}$	32.9	1.392	1.430, 1.432	1.391	1.431, 1.431	1.391	1.431, 1.431	0
$[Hf^{IV}(bpy^{\bullet})_2(bpy^{2-})]^0$	38.9	1.424	1.399, 1.398	1.418	1.404, 1.404	1.426	1.397, 1.397	0
$[Hf^{IV}(bpy^{2-})_2(bpy^{\bullet})]^{1-}$	39.0	1.406	1.415, 1.415	1.407	1.415, 1.414	1.405	1.415, 1.416	$^1/_2$
$[Hf^{IV}(bpy^{2-})_3]^{2-}$	37.2	1.390	1.433, 1.433	1.390	1.434, 1.433	1.390	1.433, 1.433	0
$[Nb^{IV}(bpy^{\bullet})_2(bpy^{2-})]^0$	45.4	1.435	1.390, 1.390	1.437	1.389, 1.387	1.436	1.388, 1.389	$^1/_2$
$[Nb^{IV}(bpy^{2-})_2(bpy^{\bullet})]^{1-}$	44.0	1.415	1.407, 1.407	1.418	1.404, 1.403	1.418	1.403, 1.403	0
$[Ta^{V}(bpy^{2-})_2(bpy^{\bullet})]^0$	41.5	1.420	1.405, 1.396	1.421	1.405, 1.395	1.420	1.405, 1.396	$^1/_2$
$[Ta^{V}(bpy^{2-})_3]^{1-}$	38.8	1.400	1.425, 1.411	1.400	1.425, 1.411	1.400	1.425, 1.411	0

[a]Average twist angle Θ (deg). [b]Ground state. [c]Calculation performed using COSMO(water) (i.e., the solvent dielectric of water).

dx.doi.org/10.1021/ic302799s | Inorg. Chem. 2013, 52, 2242−2256

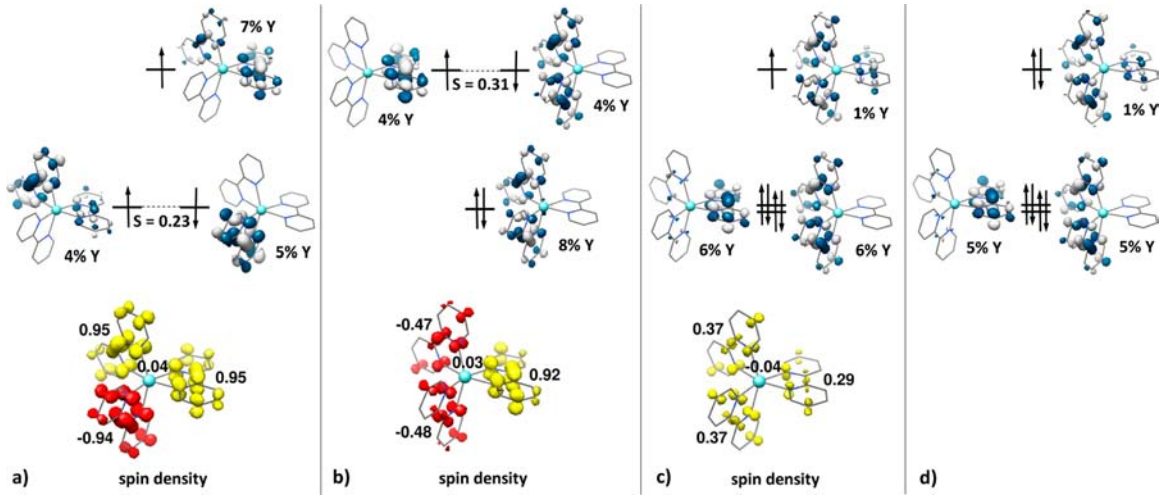

Figure 6. Frontier orbitals and spin density plots (yellow, α-spin; red, β-spin) with Mulliken spin populations obtained from DFT calculations for (a) $[Y^{III}(bpy^{\bullet})_3]^0$ ($S = {}^1/_2$), (b) $[Y^{III}(bpy^{\bullet})_2(bpy^{2-})]^{1-}$ ($S = 0$), (c) $[Y^{III}(bpy^{\bullet})(bpy^{2-})_2]^{2-}$ ($S = {}^1/_2$), and (d) $[Y^{III}(bpy^{2-})_3]^{3-}$ ($S = 0$).

such that one bore 0.93 α-, another 0.90 β-, and the third 0.05 β-spins. This is reflected in the structural parameters of the bpy ligands (Table 7) with $C_{py}-C_{py}$ distances of 1.436, 1.433, and 1.398 Å, respectively. Spin localization of this type upon application of COSMO(water) was previously observed in DFT calculations for closely related Cr complexes.[52] *J*-values for antiferromagnetic coupling between the two electrons located on the bpy ligands in $[Y(bpy)_3]^{1-}$ were calculated to be -230 and -135 cm^{-1} in the gas and liquid phases, respectively. Thus, an electronic structure description as in $[Y^{III}(bpy^{\bullet})_2(bpy^{2-})]^{1-}$ ($S = 0$) may be envisaged, though it is uncertain whether the unpaired spin density is localized or not. It should be noted that once again the geometry of the YN_6 polyhedron in the monoanion is distorted octahedral ($\Theta = 38°$ in both gas and liquid phase calculations, Table 7).

A UKS calculation for the dianion $[Y(bpy)_3]^{2-}$ ($S = {}^1/_2$) revealed the presence of three nearly equivalent reduced bpy ligands, which would suggest that the single unpaired electron is delocalized over all three ligands, $(bpy_3)\}^{5\bullet}$. Indeed, the Mulliken spin population analysis (Figure 6) shows one unpaired electron delocalized over three equivalent bpy ligands and, once again, zero spin density at the metal ion. In addition, the twist angle ($\Theta = 38°$) is consistent with a d^0 central metal atom (Table 7). Hence, the electronic structure of the dianion is best described as $[Y^{III}(bpy^{2-})_2(bpy^{\bullet})]^{2-}$ ($S = {}^1/_2$).

The last member of this series is the diamagnetic trianion. The RKS geometry optimized structure revealed the presence of three equivalent $(bpy^{2-})^{2-}$ ligands and a distorted octahedral YN_6 polyhedron ($\Theta = 37°$). Thus, its electronic structure is best described as $[Y^{III}(bpy^{2-})_3]^{3-}$. Consistent with this notion the qualitative MO diagram shows five unoccupied metal d-orbitals (Y character ~80%) at high energy and three doubly occupied ligand-centered orbitals (i.e., $3 \times (bpy^{2-})^{2-}$) with <5% Y character (Figure S18).

$[Ti(bpy)_3]^n$ (n = 1+, 0, 1−, 2−, 3−) Series. The titanium series begins with the recently synthesized and characterized monocation.[48] We have optimized the geometry of the $S = {}^1/_2$ ground and $S = {}^3/_2$ excited states, with the UKS solution for the latter being ~7 kcal mol^{-1} higher in energy than the former. Notably, the $S = {}^1/_2$ UKS calculation underwent spontaneous symmetry breaking to yield a BS(2,1) solution. As expected, on the basis of the large energy gap between the $S = {}^1/_2$ and $S = {}^3/_2$ UKS solutions, performing a BS(2,1) single point calculation yielded a large *J*-value of -693 cm^{-1}. The ground state BS(2,1) geometry optimized structure exhibited a nearly octahedral ($\Theta = 48°$) TiN_6 polyhedron containing three nearly identical bpy ligands with average $C_{py}-C_{py}$ and C−N distances of 1.451 and 1.371 Å, respectively. These values are in excellent agreement with those obtained from the arithmetic mean of two uncoordinated $(bpy^{\bullet})^{1-}$ radical anions and one neutral (bpy^0) (1.451 and 1.374 Å, respectively, see Table 7) and point to a $(bpy_3)^{2-}$ ligand unit. Hence, the electronic structure of the monocation may then be best described as $[Ti^{III}(bpy^{\bullet})_2(bpy^0)]^{1+}$ ($S = {}^1/_2$), with the ground state resulting from a strong antiferromagnetic coupling between a Ti^{III} ion and a π radical $(bpy^{\bullet})^{1-}$ anion, which is corroborated by a Mulliken spin density population of 1.22 at the titanium center (see Figure S3). However, this simple electronic picture is somewhat muddied by extensive covalency, which manifests in an overlap integral of 0.77 between the antiferromagnetically coupled spin orbitals and significant Ti-character of the α-spin orbitals (Figure S19). As a consequence it is difficult to accurately assign a Ti oxidation state, but it would be best to describe the $[Ti^{III}(bpy^{\bullet})_2(bpy^0)]^{1+}$ ($S = {}^1/_2$) ground state as containing significant Ti^{II} character. Regardless, this result excludes a +IV central ion.

On the basis of its experimentally observed diamagnetism at 300 K,[8] DFT calculations for the neutral complex $[Ti(bpy)_3]^0$ were performed using the RKS and BS(2,2) formalisms. Additionally, the $S = 1$ excited state was probed using the UKS and BS(3,1) formalisms, and found to converge to identical solutions (i.e., the former underwent spontaneous symmetry breaking). The single point energies obtained from initial calculations for all solutions were within 2 kcal mol^{-1} of one another (i.e., effectively isoenergetic), but with the $S = 1$ spin state lowest in energy and the BS(2,2) solution only 0.6 kcal mol^{-1} below the RKS solution (Table S14). This outcome defies experimental observations, expectations based upon Goodenough−Kanamori rules,[53] and the fact that the *J*-value obtained for the BS(2,2) calculation of -201 cm^{-1} was of greater magnitude than the value of -145 cm^{-1} obtained in the BS(3,1) calculation. In response the single point calculations were repeated incorporating a dispersion forces correction,[32] which yielded an energetic ordering in line with experiment and

dx.doi.org/10.1021/ic302799s | *Inorg. Chem.* 2013, 52, 2242−2256

our expectations (Table S15). More specifically, the BS(2,2) solution was found to be lowest in energy. However, all solutions were still within 2 kcal mol^{-1} of one another, which would seem to defy experimental observations because, on the basis of the DFT results, we might expect partial occupation of the S = 1 excited state at room temperature. This is not the case, so we can conclude that the DFT protocol used struggles to accurately model the relative energies of the various electronic states of $[Ti(bpy)_3]^0$.

In the BS(2,2) solution, the lowest energy state that conforms to experimental observations of an S = 0 ground state, the average calculated intraligand $C_{py}-C_{py}$ and C−N bond distances in the three bpy ligands are nearly identical (Table 7) at 1.427 and 1.385 Å, respectively. Additionally, the twist angle in the TiN_6 polyhedron Θ of 46° is at the octahedral limit (Table 7). Furthermore, the aforementioned bond distances are essentially the same in the RKS and S = 1 excited state optimized geometries (Table S2), all of which point to the presence of three π radical monoanions $(bpy^{\bullet})^{1-}$ in all cases. Hence, the central titanium ion has a +III oxidation state (d^1 electron configuration), and its electronic structure is best described as $[Ti^{III}(bpy^{\bullet})_3]^0$ (S = 0), as was proposed by previous authors.[8i] The S = 0 ground state is then attained via one strong antiferromagnetic metal−ligand π radical exchange coupling and an antiferromagnetic ligand radical−radical coupling facilitated via an empty metal t_{2g} orbital in accordance with the Goodenough−Kanamori description for such a superexchange pathway.[53] The qualitative MO diagram for the BS(2,2) solution, shown in Figure S21, is in accordance with this picture and also contains four unoccupied metal d-orbitals, as expected for a Ti^{III} ion. (Note that the corresponding qualitative MO diagram for the BS(3,1) S = 1 excited state lacks the antiferromagnetic metal−ligand π radical exchange interaction seen in the BS(2,2) solution, but is otherwise qualitatively identical and is also consistent with the Ti ion possessing a +III oxidation state.) A Mulliken spin population analysis for the BS(2,2) solution yields 0.70 α-spins at the Ti center, a further 0.48 α-spins on one bpy, and 2 × 0.59 β-spins on the two remaining bpy ligands. Notably, these values do not amount to 4 unpaired spins, a situation that results from high levels of covalency and is reflected in observation of large overlap integrals for the spin orbitals involved in the two coupling pathways (0.80 and 0.76 for Ti−$bpy^{\bullet}$ and $bpy^{\bullet}$−$bpy^{\bullet}$, respectively).

Upon reduction of the neutral species, one might expect addition of an electron to one of the bpy π^* orbitals to yield a dianion, leaving the remaining unpaired electrons on the Ti^{III} center and the two $(bpy^{\bullet})^{1-}$ to antiferromagnetically couple, thereby yielding an $S = {}^1/_2$ ground state. In agreement with these expectations, the fluid THF solution EPR spectrum of the monoanion $[Ti(bpy)_3]^{1-}$ has been reported to display a narrow isotropic signal at g_{iso} = 2.0074 ± 0.0002 with no resolvable Ti hyperfine,[8e] suggestive of a ligand-centered $S = {}^1/_2$ spin system. However, DFT calculations performed using the BS(2,1) formalism yielded solutions in which the two $(bpy^{\bullet})^{1-}$ ligands antiferromagnetically couple to one another leaving the unpaired electron on the Ti^{III} center (Figures S5 and S22).

Interestingly, the corresponding $S = {}^1/_2$ UKS calculation converges not to the BS(2,1) solution, but to a BS(3,2) one (Figure S23) that is 3 kcal mol^{-1} lower in energy (Table S14). Therein the α-spin orbitals are clearly ligand centered, containing <10% Ti character in all cases, and the two β-spin orbitals both contain just over 50% Ti character. Importantly, this solution contains a ligand-centered unpaired electron. The moderate Ti-character of the β-spin orbitals and the large overlap integrals (>0.8) associated with the antiferromagnetic interactions with the corresponding α-spin orbitals are characteristic of high levels of covalency, which complicates efforts to assign an oxidation state to the Ti center. However, a Mulliken spin population analysis for this BS(3,2) ground state solution contains a total of +2.11 unpaired spins delocalized over the three bpy ligands and −1.11 unpaired spins on the Ti center. On this basis, formulation as $[Ti^{III}(bpy^{2-})(bpy^{\bullet})_2]^{1-}$ seems reasonable, but with a contribution of some Ti^{II} character. In support of this notion, the average calculated $C_{py}-C_{py}$ and C−N distances of 1.411 and 1.398 Å, respectively, for the $S = {}^1/_2$ UKS geometry optimized structure are significantly shorter and longer than those of the neutral species at 1.427 and 1.385 ÅÅ, respectively. Additionally, the twist angle (Θ = 45°) remains close to the octahedral limit. All of this is consistent with ligand-centered reduction and retention of a +III oxidation state at Ti.

The two subsequent one-electron reductions of the monoanionic species yield the corresponding dianion, $[Ti(bpy)_3]^{2-}$, and trianion, $[Ti(bpy)_3]^{3-}$, which possess S = 0 and $S = {}^1/_2$ ground states, respectively. For the dianion a BS(1,1) single point calculation using the corresponding geometry optimized structure yielded a solution with a J-value of −478 cm^{-1} that is only 1.1 kcal mol^{-1} lower in energy than the corresponding RKS solution. In this case, the energetic proximity of the BS(1,1) and RKS solutions derives from the poor spatial overlap of the constituent orbitals involved in the antiferromagnetic interaction in the former (overlap integral ∼0.0). As shown in Table 7 the di- and trianions both contain three nearly equivalent bpy ligands (i.e., the unpaired spin is delocalized over all three bpy ligands). The average $C_{py}-C_{py}$ distances of 1.40 Å in the dianion and 1.38 Å in the trianion (the corresponding average C−N distances are 1.44 and 1.43 Å, respectively) are consistent with successive one-electron reduction of the bpy ligands and not the Ti^{III} center. This proposition is supported by the calculated Mulliken spin populations (Figures S6 and S7) and qualitative MO diagrams (Figures S24 and S25), yielding the electronic descriptions $[Ti^{III}(bpy^{2-})_2(bpy^{\bullet})]^{2-}$ and $[Ti^{III}(bpy^{2-})_3]^{3-}$. Hence, the S = 0 ground state in the former case is most probably obtained via antiferromagnetic metal−ligand π radical exchange coupling, and the $S = {}^1/_2$ ground state in the latter is due to a single Ti-centered unpaired electron.

Remarkably, the calculated average Ti−N bond lengths do not vary greatly over the series of five complexes, being shortest in the neutral species at 2.12 Å and longest in the trianion at 2.19 Å, which is consistent with the central Ti ion retaining a +III (d^1) oxidation state throughout and indicates that these complexes differ only in the charge distributed over the three bpy ligands.

$[M(bpy)_3]^n$ (M = Zr, Hf and n = 0, 1−, 2−) Series. Calculation of the geometry optimized structure of $[Zr(bpy)_3]^0$ yields a starkly different structure/electronic description than that obtained for $[Ti(bpy)_3]^0$, even though both species possess an S = 0 ground state. As can be seen from the data in Table 7, the three nearly equivalent bpy ligands in $[Zr(bpy)_3]^0$ are more reduced (the average C−N distance in $[Zr(bpy)_3]^0$ is calculated to be 1.396 versus 1.385 Å for its Ti analogue), which concomitantly implies a higher degree of oxidation at the central metal ion. From this we can infer that the central Zr ion possesses a +IV oxidation state. In the resulting

dx.doi.org/10.1021/ic302799s | Inorg. Chem. 2013, 52, 2242−2256

$[Zr^{IV}(bpy^{\bullet})_2(bpy^{2-})]^0$ electronic description the observed $S = 0$ ground state would derive from intramolecular antiferromagnetic coupling of the two ligand π radicals.

The aforementioned picture is confirmed by the schematic MO scheme for the BS(1,1) solution shown in Figure S27, which contains five unoccupied Zr d-orbitals, two antiferromagnetically coupled ligand centered SOMOs ($J_{calcd} = -1012$ cm^{-1}) corresponding to two $(bpy^{\bullet})^{1-}$ radicals, and the doubly occupied ligand-centered π orbital of the dianion $(bpy^{2-})^{2-}$ (HOMO). A Mulliken spin population analysis of the BS(1,1) solution (Figure S8) exhibits near zero unpaired spin at the central Zr ion, +0.54 unpaired spins at one bpy ligand, −0.42 at the second, and −0.13 at the third. Interestingly, application of a strong solvent dielectric in the form of COSMO(water) causes greater localization of the spin density, such that two of the ligands exhibit a Mulliken spin population of ∼0.55 unpaired spins (one with α-spin and the other β-spin) and the third carries only −0.04 (Figure S13). This is reflected in the structural parameters of the bpy ligands, which display $C_{py}-C_{py}$ distances of 1.435 and 1.413 Å, respectively. However, it should be noted that the BS(1,1) solution is only 0.3 kcal mol^{-1} lower in energy than the RKS solution, $[Zr^{IV}(bpy^{2-})_2(bpy^0)]^0$. This is a direct result of the extensive covalency, which is also reflected in the significant incorporation of Zr-character in to the ligand-based frontier orbitals (Figures S27 and S28) and the large overlap integral between the antiferromagnetically coupled SOMOs in the BS(1,1) solution. As a consequence it is not possible to discern between the two resonance forms $[Zr^{IV}(bpy^{2-})_2(bpy^0)]^0$ and $[Zr^{IV}(bpy^{\bullet})_2(bpy^{2-})]^0$.

Calculations for the neutral species $[Hf(bpy)_3]^0$ revealed similar results to those obtained for $[Zr(bpy)_3]^0$. Once again, a d^0 metal center (i.e., Hf^{IV}) carrying no spin density (Figure S9) was identified, leading to the analogous electronic description $[Hf^{IV}(bpy^{\bullet})_2(bpy^{2-})]^0$. Additionally, the calculated radical−radical spin exchange coupling constant $J_{calcd} = -940$ cm^{-1} is similar in magnitude to that found for the Zr analogue. Furthermore, the BS(1,1) solution is only 0.5 kcal mol^{-1} lower in energy than the corresponding RKS solution $[Hf^{IV}(bpy^{2-})_2(bpy^0)]$, once again reflecting the large overlap integral (in this case 0.73) between the antiferromagnetically coupled SOMOs. In close analogy to $[Zr(bpy)_3]^0$, the HfN_6 polyhedron is also calculated to be a distorted octahedron ($\Theta = 39°$).

Geometry optimization of the mono- and dianions $[Zr(bpy)_3]^{1-,2-}$ and $[Hf(bpy)_3]^{1-,2-}$ yields in all cases structures containing three equivalent (bpy) ligands and average twist angles of a distorted octahedron (39° and 37° for the mono- and dianionic Hf complexes, respectively, and 33° for both Zr complexes). On the basis of the structural parameters of their geometry optimized structures, the ligands in the two monoanions possess a $(bpy_3)^{5-\bullet}$ ligand unit and +IV metal ion. The Mulliken spin density population analysis for the monoanions (Figures S8 and S9) is in good agreement with this interpretation, with there being very little spin density located at the central Zr^{IV} and Hf^{IV} ions (−0.18 and −0.12 unpaired spins, respectively) and a total of +1.18 and +1.11 unpaired spins, respectively, delocalized over the ligands ($S = {}^1/_2$ ground state). The electronic structures of the monoanions are thus best described as $[Zr^{IV}(bpy^{\bullet})(bpy^{2-})_2]^{1-}$ and $[Hf^{IV}(bpy^{\bullet})(bpy^{2-})_2]^{1-}$. Indeed, the qualitative MO schemes (Figures S29 and S32) each display 5 unoccupied metal d-orbitals at high energy, a ligand-based SOMO of a $(bpy^{\bullet})^{1-}$ radical anion, and two ligand-based HOMO's of two $(bpy^{2-})^{2-}$ dianions at lower energy.

The RKS optimized geometries of the diamagnetic dianions $[Zr(bpy)_3]^{2-}$ and $[Hf(bpy)_3]^{2-}$ (no BS solutions were found) both display three equivalent $(bpy)^{2-}$ dianions, thereby rendering the central metal ions Zr^{IV} and Hf^{IV}. This is reflected in the metric parameters of both geometry optimized structures (Table 7) and their qualitative MO diagrams (Figures S30 and S33), which contain five unoccupied metal d-orbitals at high energy and three ligand-based HOMOs that correspond to a full set of $(bpy^{2-})^{2-}$ dianions. Notably, the optimized geometry of $[Zr^{IV}(bpy^{2-})_3]^{2-}$ ($S = 0$) is in excellent agreement with the experimental structure,[15] including the calculated and experimental average twist angles ($\Theta = 33°$ in both cases).

$[M(bpy)_3]^n$ (M = V, Nb, Ta and n = 0, 1−) Series. In a recent study, we experimentally verified that neutral $[V(bpy)_3]^0$ possesses the electronic structure $[V^{II}(bpy^{\bullet})_2(bpy^0)]^0$, fully corroborated by DFT calculations, in which the α-spins of a central V^{II} d^3 ion couple antiferromagnetically to two ligand π radical anions (β-spins) to give an $S = {}^1/_2$ ground state ($J_{calcd} = -651$ cm^{-1}).[21b] The remaining unpaired electron resides in a metal-centered d_{z^2} orbital, a fact confirmed experimentally by EPR spectroscopy. For the analogous diamagnetic monoanion it was shown that an electronic structure $[V^{II}(bpy^{\bullet})_3]^{1-}$ prevails, wherein the central V^{II} ion is intramolecularly antiferromagnetically coupled to three $(bpy^{\bullet})^{1-}$ radical anions,[21b] thereby affording the observed $S = 0$ ground state.

Interestingly, the analogous $[Nb(bpy)_3]^0$ and $[Ta(bpy)_3]^0$ complexes also both exhibit an $S = {}^1/_2$ ground state but different electronic structures than their vanadium analogue. The UKS geometry optimized structure of $[Nb(bpy)_3]^0$ contains three equivalent ligands wherein the average C−N distance is somewhat longer than observed in $[V^{II}(bpy^{\bullet})_2(bpy^0)]$ ($S = {}^1/_2$), which is indicative of a more reduced set of bpy ligands and a higher metal oxidation state in the former. (Attempts to calculate BS solutions, such as BS(2,1) or BS(3,2), for the neutral species $[Nb(bpy)_3]^0$ were unsuccessful with all calculations converging to the UKS solution described below.) The average twist angle in the NbN_6 polyhedron of 45° is effectively octahedral. Thus, $[Nb^{IV}(bpy^{\bullet})_2(bpy^{2-})]^0$ or $[Nb^{III}(bpy^{\bullet})_3]^0$ are reasonable propositions for the electronic structures of this neutral species. The presence of a LLIVCT band in the IR spectrum of $[Nb(^tbpy)_3]^0$ requires that this complex display ligand mixed-valency, which precludes the latter Nb^{III} containing electronic description. Assuming the former electronic description is correct, a BS(2,1) solution leaving the unpaired electron on the ligand might be expected to exist. However, our EPR results indicate that the unpaired electron is located in a metal d_{z^2} orbital, so description of the electronic structure as $[Nb^{IV}(bpy^{\bullet})_2(bpy^{2-})]^0$ appears *not* to agree with experiment.

Therefore, we suggest an electronic structure in which the energetic separation between the ligand-derived e and a_2 orbitals is sufficiently large that the latter remains unoccupied, thereby locating the unpaired electron at the Nb center. This situation can be thought of as $[Nb^{IV}(bpy^{2-})_2(bpy^0)]^0$ ($S = {}^1/_2$), where a central Nb^{IV} d^1 ion, two diamagnetic $(bpy^{2-})^{2-}$, and a neutral diamagnetic (bpy^0) ligand are present. The average calculated $C_{py}-C_{py}$ distance of 1.42 Å would fit this description (two $(bpy^{2-})^{2-}$ at 1.40 Å and one bpy^0 at 1.47 Å), as would the calculated average C−N bond length of 1.39 Å (1.42 Å in $(bpy^{2-})^{2-}$, and 1.35 Å in bpy^0). The Mulliken spin population analysis shown in Figure 7 corroborates this description: the

dx.doi.org/10.1021/ic302799s | Inorg. Chem. 2013, 52, 2242−2256

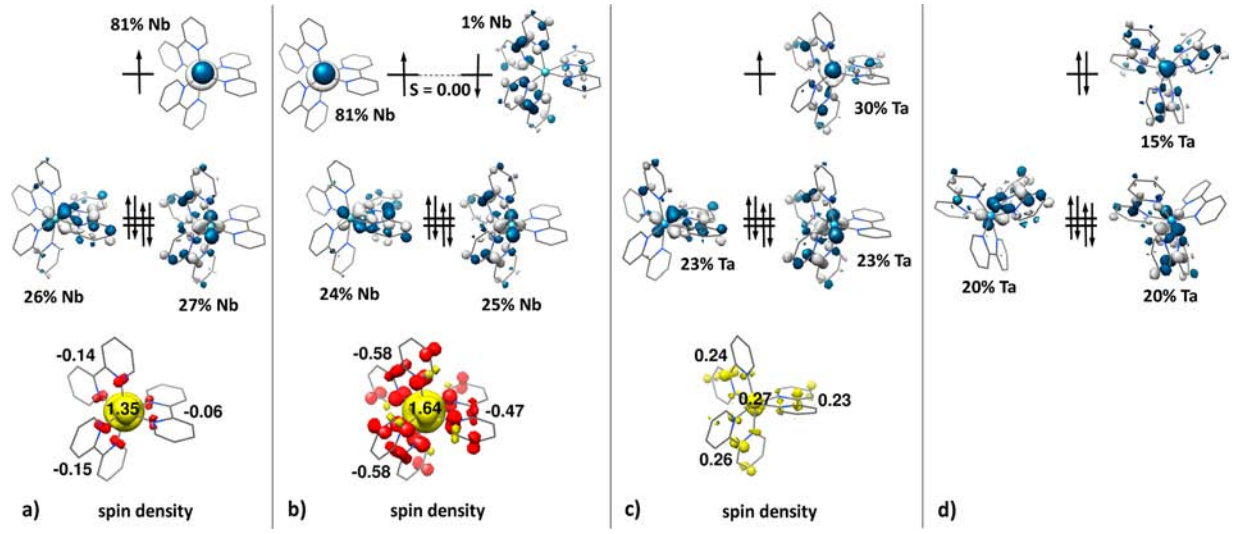

Figure 7. Frontier orbitals and spin density plots (yellow, α-spin; red, β-spin) with Mulliken spin populations obtained from DFT calculations for (a) $[Nb^{IV}(bpy^{\bullet})_2(bpy^{2-})]^0$ ($S = {}^1/_2$), (b) $[Nb^{IV}(bpy^{\bullet})(bpy^{2-})_2]^{1-}$ ($S = 0$), (c) $[Ta^{V}(bpy^{\bullet})(bpy^{2-})_2]^0$ ($S = {}^1/_2$), and (d) $[Ta^{V}(bpy^{2-})_3]^{1-}$ ($S = 0$).

central Nb ion possesses +1.35 and the three bpy ligands carry a total of −0.35 unpaired spins. Accordingly, the corresponding qualitative MO scheme in Figure S34 displays a metal-centered d_{z^2} SOMO (nonbonding character), four unoccupied metal-centered d-orbitals (>58% Nb character), two occupied ligand-centered MOs, and an unoccupied ligand-centered orbital a_2 (LUMO).

The electronic structure of the corresponding neutral complex $[Ta(bpy)_3]^0$ ($S = {}^1/_2$) is calculated to be strikingly different from that of its niobium analogue. (Note that efforts to find BS solutions were unsuccessful with all calculations converging to the UKS solution described subsequently.) Three approximately equivalent bpy ligands were found with each bearing between +0.23 and +0.26 unpaired spins (Figure 7), leaving only +0.27 unpaired spins at the Ta center. The average calculated $C_{py}-C_{py}$ bond length of 1.420 Å is significantly shorter than that in the niobium analogue (1.436 Å), which suggests that the bpy ligands have more reduced character in the former and that correspondingly the Ta center is more oxidized. Hence, the electronic structure of this complex is best formulated as $[Ta^{V}(bpy^{2-})_2(bpy^{\bullet})]^0$, which contains a Ta^{V} d^0 ion, two $(bpy^{2-})^{2-}$, and one $(bpy^{\bullet})^{1-}$. In accordance with this description the qualitative MO scheme for $[Ta(bpy)_3]^0$ (Figure S36) displays a ligand-centered a_2 SOMO, two ligand-centered HOMOs, and five virtual metal-centered d-orbitals (>55% Ta character).

The spectral and structural data detailed in this report are for complexes ligated by ^{t}bpy, not simple bpy. In an effort to probe the influence of the *tert*-butyl substituents upon the electronic structures of these complexes, we also performed DFT calculations for $[Ta(^tbpy)_3]^{0,1-}$ (see the Supporting Information for details). Interestingly, the structural parameters calculated for $[Ta(^tbpy)_3]^0$ do not deviate significantly from those found for $[Ta^{V}(bpy^{2-})_2(bpy^{\bullet})]^0$ (Tables S8 and 7, respectively). Additionally, the Mulliken spin population analysis yields between +0.28 and +0.31 unpaired spins on each ^{t}bpy ligand and a further +0.12 unpaired spins at the Ta center (Figures S12), which is very similar outcome to that for $[Ta^{V}(bpy^{2-})_2(bpy^{\bullet})]^0$, albeit with reduced spin density at the Ta center. Hence, substitution of the bpy rings with *tert*-butyl substituents appears to have no effect upon the electronic structure of neutral Ta species, and the best description of the electronic structure of the ^{t}bpy complex is also $[Ta^{V}(^tbpy)_2(^tbpy^{\bullet})]^0$. The qualitative frontier MO diagram for this complex confirms this assignment (Figure S38).

Geometry optimizations of the diamagnetic ($S = 0$) monoanions $[Ta(bpy)_3]^{1-}$ and $[Ta(^tbpy)_3]^{1-}$ have been successfully carried out using the RKS formalism (efforts to locate BS solutions were unsuccessful). In both cases, three equivalent diamagnetic $(bpy^{2-})^{2-}$ species coordinated to a diamagnetic tantalum(V) ion were found. Interestingly, all the structural peculiarities of the experimental structure are faithfully reproduced in these calculations, including (a) the short average $C_{py}-C_{py}$ bond distance of 1.40 Å and the relatively long average C−N bond length of 1.42 Å typical for $(bpy^{2-})^{2-}$ dianions; and (b) the five-membered chelate rings not possessing C_2 or σ symmetry, such that the two Ta−N distances differ by an average of 0.077 and 0.073 Å and the two C−N distances per chelate ring by 0.014 and 0.013 Å in $[Ta(bpy)_3]^{1-}$ and $[Ta(^tbpy)_3]^{1-}$, respectively. The corresponding experimental values are 0.064 and 0.011 Å, respectively. It is notable that these unusual structural features are reproduced in gas phase DFT calculations regardless of whether the bpy ligands have *tert*-butyl substituents or not, which suggests that they can be attributed to electronic factors and do not derive from sterics or crystal packing forces. In contrast, the calculated and experimental structures both display distorted octahedral geometries, but the twist angle Θ in the former case (38−39°) is noticeably larger than in the latter case (32°). The reason for this disparity is unclear, but it may be due to a shallow potential energy surface associated with this geometric distortion or an inability of DFT to accurately model the interaction stemming from the close contact between neighboring bpy rings observed in the X-ray structure. In accordance with the electronic structure inferred from the structural picture described above, the qualitative MO schemes for $[Ta(bpy)_3]^{1-}$ and $[Ta(^tbpy)_3]^{1-}$ (Figures S37 and S39, respectively) display five unoccupied metal d-orbitals (>54% Ta) and three ligand-based doubly occupied π orbitals. Thus, the electronic structures of these monoanions are best described as $[Ta^{V}(bpy^{2-})_3]^{1-}$ and $[Ta^{V}(^tbpy^{2-})_3]^{1-}$.

dx.doi.org/10.1021/ic302799s | *Inorg. Chem.* 2013, 52, 2242−2256

In contrast, $[Nb(bpy)_3]^{1-}$ has a BS(1,1) solution 7.3 kcal mol^{-1} lower in energy than the RKS one. Therefore, the former is the ground state in this case, so subsequent discussions will focus on this solution. (Note that all other broken symmetry calculations BS(1,1), BS(2,2), and BS(3,3) converged to the aforementioned BS(1,1) solution.) In the geometry optimized structure the three bpy chelate rings were found to be equivalent and the average calculated $C_{py}-C_{py}$ and chelate ring C−N bond lengths of 1.417 and 1.405 Å, respectively, point to a delocalized distribution of two $(bpy^{2-})^{2-}$ and one $(bpy^{\bullet})^{1-}$, thereby implicating $[Nb^{IV}(bpy^{2-})_2(bpy^{\bullet})]^{1-}$ as the electronic structure. In accordance with this inference, the qualitative MO diagram (Figure S35) contains four unoccupied d-orbitals, a singly occupied d_{z^2} orbital antiferromagnetically coupled to a ligand-based SOMO (J_{calcd} = −1217 cm^{-1}), and two doubly occupied ligand-based orbitals that correspond to $(bpy^{2-})^{2-}$ ligands. Notably, the $(bpy^{2-})^{2-}$ orbitals contain a relatively large amount of metal d-character (ca. 25%), which is indicative of the high levels of covalency seen for second and third row transition metals. This combined with the strong π-donor properties of the $(bpy^{2-})^{2-}$ ligand result in a distortion of the spin density distribution (Figure 7) that manifests in a Mulliken spin population of +1.64 on the Nb center, which can be viewed as a significant introduction of Nb^{III} character.

DISCUSSION

In a previous paper we demonstrated computationally that the electronic structures of the neutral complexes $[Al(bpy)_3]^0$ and $[Sc(bpy)_3]^0$ are best described as species containing a central trivalent metal ion (Al^{III}, Sc^{III}) and three *N,N′*-coordinated $(bpy^{\bullet})^{1-}$ radical anions, namely $[Al^{III}(bpy^{\bullet})_3]^0$ and $[Sc^{III}(bpy^{\bullet})_3]^0$.[21c] Both possess an $S = {}^1/_2$ ground state and an energetically close lying $S = {}^3/_2$ excited state. Thus, the three $(bpy^{\bullet})^{1-}$ radical anions are intramolecularly antiferromagnetically coupled, as has been established experimentally by temperature-dependent magnetic susceptibility measurements and EPR.[50,51] Additionally, the agreement between calculated and experimentally determined exchange coupling constants and geometrical features of the bpy ligands is excellent. It is quite reasonable that the calculated electronic structure of the corresponding neutral species of yttrium is similar and is best described as $[Y^{III}(bpy^{\bullet})_3]^0$, with an $S = {}^1/_2$ ground and an $S = {}^3/_2$ excited state (J_{calcd} = −108 cm^1). No experimental data (spectroscopic or structural) are available for comparison, but the reported magnetic moment of 1.84 μ_B[54] measured at ambient temperature is consistent with an $S = {}^1/_2$ ground state resulting from an intramolecular antiferromagnetic coupling between three $(bpy^{\bullet})^{1-}$ radical anions.

Complexes containing three equivalent diamagnetic dianionic $(bpy^{2-})^{2-}$ ligands have been identified computationally and/or experimentally in this work in the following species: $[Y^{III}(bpy^{2-})_3]^{3-}$ (S = 0); $[Ti^{III}(bpy^{2-})_3]^{3-}$ ($S = {}^1/_2$); $[Zr^{IV}(bpy^{2-})_3]^{2-}$ (S = 0); $[Hf^{IV}(bpy^{2-})_3]^{2-}$ (S = 0); and $[Ta^{V}(bpy^{2-})_3]^{1-}$ (S = 0). The same conclusion was previously reached computationally for $[Cr^{III}(bpy^{2-})_3]^{3-}$ ($S = {}^3/_2$),[21a] and in all cases the calculated and experimentally determined geometrical details of the chelate rings clearly define the oxidation level of the ligands as $(bpy^{2-})^{2-}$. This is also true for the geometry optimized structure of diamagnetic $[Al^{III}(bpy^{2-})_3]^{3-}$ (Table 6), calculated here, in which the chelate ring containing C−C and C−N bond distances are very similar to those observed in the X-ray structure of tetrahedral $[Al^{III}(bpy^{2-})_2]^{1-}$ (S = 0).[7]

According to the present DFT calculations the paramagnetic complex $[Ti^{III}(bpy^{2-})_3]^{3-}$ ($S = {}^1/_2$) consists of a central Ti^{III} ion (d^1) and three dianions $(bpy^{2-})^{2-}$. No evidence was found for Ti^{II} a lower metal oxidation state. In addition, the dianionic Zr and Hf complexes, plus $[Ta^{V}(bpy^{2-})_3]^{1-}$, possess high-valent Zr^{IV}, Hf^{IV}, and Ta^{V} ions. Again we have not found evidence (experimental or computational) for lower oxidation states of these metal ions, though high levels of covalency in these complexes makes oxidation state assignment less reliable. In contrast, DFT calculations for $[V(bpy)_3]^{3-}$ (S = 1) have shown that its electronic structure is best described by resonance structures $\{[V^{II}(bpy^{2-})_2(bpy^{\bullet})]^{3-} \leftrightarrow [V^{III}(bpy^{2-})_3]^{3-}\}$,[21b] and confirmed a +III central ion in $[Cr^{III}(bpy^{2-})_3]^{3-}$ ($S = {}^3/_2$).[21a]

In the following section we will briefly discuss the qualitative MO schemes for the early transition metal complexes calculated in this work (see Supporting Information). For all complexes a twist angle Θ smaller than ∼50° was found, indicative of a distorted octahedral geometry (D_3 symmetry) resulting in the splitting of the metal centered t_{2g} set (in O_h symmetry) into an e set and an $a_1(d_{z^2})$ orbital of >50% metal character. There are three ligand-based orbitals, e and a_2, which are empty in $[(bpy^0)_3]^0$, singly occupied in $[(bpy^{\bullet})_3]^{3-}$, and fully occupied in $[(bpy^{2-})_3]^{6-}$. As it turns out the second and third row transition metal ions Y, Zr, Hf, and Ta possess a stable electronic configuration with five unoccupied energetically high lying metal d-orbitals. (Nb is the exception here because it possesses a d^1 electronic configuration.) The ligand e and a_2 orbitals are greatly stabilized with respect to the d-orbitals and are therefore occupied in these series.

Consequently, all species of the series $[Y^{III}(bpy)_3]^{0,1-,2-,3-}$ shown in Figure 6 possess an Y^{III} d^0 central ion, and upon moving from the neutral complex containing three $(bpy^{\bullet})^{1-}$ radical anions, there is a progressive occupation of the ligand orbitals to eventually produce three $(bpy^{2-})^{2-}$ dianions in the trianion. The complexes containing two or more $(bpy^{\bullet})^{1-}$ anions display relatively weak intramolecular antiferromagnetic coupling between the radical anions. Thus, calculations allow assignment of the electronic structures as $[Y^{III}(bpy^{\bullet})_3]^0$ ($S = {}^1/_2$), $[Y^{III}(bpy^{\bullet})_2(bpy^{2-})]^{1-}$ (S = 0), $[Y^{III}(bpy^{\bullet})(bpy^{2-})_2]^{2-}$ ($S = {}^1/_2$), and $[Y^{III}(bpy^{2-})_3]^{3-}$ (S = 0). The Mulliken spin population analysis is in accord with this result, with all complexes having virtually no (<0.04) spin density at the metal ions. One unpaired electron resides on each $(bpy^{\bullet})^{1-}$ ligand in the neutral species (one β- and two α-spins for the $S = {}^1/_2$ ground state, and three α-spins in the excited $S = {}^3/_2$ state). The two ligand mixed-valent species, namely the monoanionic and dianionic species, display spin density on all three ligands. More specifically, for the monoanion in the S = 0 ground state there is α-spin of +0.92 on one of the ligands and β-spin of −0.47 and −0.48 on the other two, whereas the three bpy ligands in the S = 1 excited state (Figure S2) have 0.51, 0.68, and 0.82 unpaired spins, respectively. In the dianion the electron hole is delocalized over all three ligands. Notably, performing geometry optimizations with the inclusion of a strong solvent dielectric in the form of COSMO(water) causes some redistribution of the spin density localized on the bpy rings. However, only in the case of the BS(1,1) calculation for the monoanionic species does this lead to a fully localized structure (Figure S13), which in this case contains a $(bpy^{2-})^{2-}$ dianion and two $(bpy^{\bullet})^{1-}$ radical anions.

The successive filling of the LUMOs of the three $(bpy^{\bullet})^{1-}$ ligands upon reducing the neutral complex $[Y^{III}(bpy)_3]^0$ results in a significant linear variation of the average $C_{py}-C_{py}$ and C−

dx.doi.org/10.1021/ic302799s | Inorg. Chem. 2013, 52, 2242−2256

N distances of the M(bpy) chelates, as shown in Figure 8. Therein the average calculated $C_{py}-C_{py}$ distance decreases

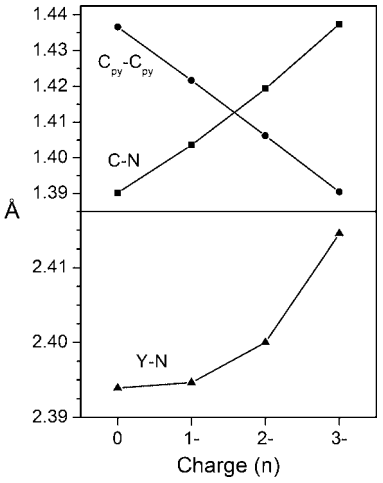

Figure 8. Top panel: Variation of the average calculated $C_{py}-C_{py}$ (●) and chelate ring C−N distances (■) for $[Y(bpy)_3]^n$ as a function of charge (n). Bottom panel: The corresponding changes in average calculated Y−N bond lengths (▲).

from 1.436 Å in the neutral species to 1.391 Å in the trianionic species, and conversely, the average C−N bond length in the chelate ring increases from 1.391 to 1.438 Å.

A very similar picture emerges for the series $[M^{IV}(bpy)_3]^{0,1-,2-}$, where M = Zr and Hf, with both metals possessing a d^0 electron configuration throughout. Hence, the electronic structures of the monoanionic and dianionic species are best described as $[M^{IV}(bpy^{2-})_2(bpy^{\bullet})]^{1-}$ ($S = {}^1/_2$) and $[M^{IV}(bpy^{2-})_3]^{2-}$ ($S = 0$), respectively. The unpaired electron in the former case is calculated to be (partly) delocalized over all three bpy radicals. Both neutral species, $[M^{IV}(bpy^{\bullet})_2(bpy^{2-})]^0$ (M = Zr, Hf), possess a singlet ground state due to strong intramolecular antiferromagnetic coupling of the two $(bpy^{\bullet})^{1-}$ ligands. Probably as a direct consequence of the strength of this coupling, a higher degree of localization of the two unpaired electrons on only two of the bpy ligands is calculated. In the case of the Zr complex, the degree of localization can be further enhanced by inclusion of a strong solvent dielectric in the geometry optimization. Lastly, it should be noted that these series of complexes possess a higher degree of covalency than their first-row transition metal (Sc, Ti, V) congeners, which reflects the higher metal character in the ligand-based orbitals and vice versa.

Interestingly, the monoanionic complexes of tantalum $[Ta(bpy)_3]^{1-}$ and $[Ta(^tbpy)_3]^{1-}$ have been calculated to fit into the same scheme, with the monoanions being best described as $[Ta^V(bpy^{2-})_3]^{1-}$ and $[Ta^V(^tbpy^{2-})_3]^{1-}$ (both with a singlet ground state and a d^0 metal center). The corresponding neutral complexes $[Ta(^tbpy)_3]^0$ and $[Ta(bpy)_3]^0$ (both $S = {}^1/_2$) have Mulliken spin populations at the Ta center of +0.12 and +0.27, respectively, with the remainder of the unpaired spin distributed over the three ligands. Therefore, the electronic structures of these complexes are best described as $[Ta^V(^tbpy^{2-})_2(^tbpy^{\bullet})]^0$ and $[Ta^V(bpy^{2-})_2(bpy^{\bullet})]^0$, such that the Ta ion retains its d^0 electronic configuration and the single unpaired electron is ligand-centered. This description is consistent with the EPR spectrum of $[Ta^V(^tbpy^{2-})_2(^tbpy^{\bullet})]^0$, whose most salient feature is a g-value close to that of the free electron. A strikingly similar situation was previously reported by Etienne and co-workers for $[Ta(iPr_2\text{-dad})_3]^0$ (iPr_2-dad = 1,4-diisopropyl-1,4-diazabuta-1,3-diene), though it was interpreted as containing a formally zerovalent metal center, which displays an EPR spectrum indicative of a ligand-centered radical and intrachelate C−C and C−N bond distances consistent with a $\{(iPr_2\text{-dad})_3\}^{5-}$ charge delocalized over the ligands.[55] Hence, a spectroscopic oxidation state of +V (d^0) can be assigned to the central metal ion, in close analogy to the two Ta complexes described here.

In all cases discussed up to this point the central metal ion possesses a d^0 electron configuration, and any antiferromagnetic coupling observed was achieved between two or three $(bpy^{\bullet})^{1-}$ radical anions via the superexchange mechanism. In the remaining cases the metal ion possesses a d^1 configuration (i.e., Ti^{III} and Nb^{IV}).

Calculations of the series $[Ti(bpy)_3]^{1+,0,1-,2-,3-}$ show that to a first approximation all five complexes contain a Ti^{III} d^1 metal center and all redox processes are ligand-centered, giving $[Ti^{III}(bpy^{\bullet})_2(bpy^0)]^{1+}$ ($S = {}^1/_2$), $[Ti^{III}(bpy^{\bullet})_3]^0$ ($S = 0$), $[Ti^{III}(bpy^{2-})(bpy^{\bullet})_2]^{1-}$ ($S = {}^1/_2$), $[Ti^{III}(bpy^{2-})_2(bpy^{\bullet})]^{2-}$ ($S = 0$), and $[Ti^{III}(bpy^{2-})_3]^{3-}$ ($S = {}^1/_2$). This is corroborated by the calculated $C_{py}-C_{py}$ and C−N distances for the series shown in Figure 9, where the former *decreases* and the latter *increases*

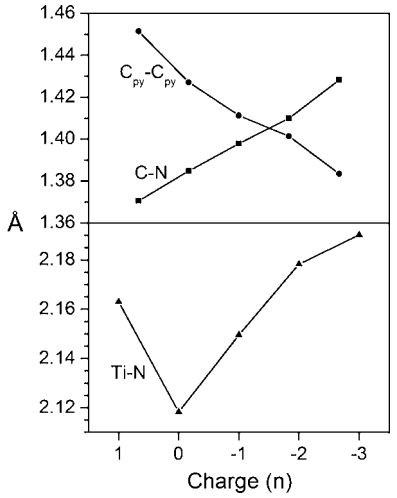

Figure 9. Top panel: Variation of the average calculated $C_{py}-C_{py}$ (●) and chelate ring C−N distances (■) for $[Ti(bpy)_3]^n$ as a function of charge (n). Bottom panel: the corresponding changes in average calculated Ti−N bond lengths (▲).

monotonically with increasing negative charge (1+, 0, 1−, 2−, 3−). The Mulliken spin population analysis reveals values for the Ti center of +1.22 for the monocation, +0.70 for the neutral species, −1.11 for the monoanion, +1.30 for the dianion, and +1.13 for the trianion, which is consistent with the presence of one unpaired electron residing at the metal center in all cases (i.e., Ti^{III}). Quite remarkably, the calculated average Ti−N bond lengths for all five species are in the narrow range 2.12−2.19 Å, which further illustrates the invariant metal oxidation state.

Finally, calculations show the Nb neutral and monoanionic species are best formulated as $[Nb^{IV}(bpy^{2-})_2(bpy^0)]^0$ ($S = {}^1/_2$) and $[Nb^{IV}(bpy^{2-})_2(bpy^{\bullet})]^{1-}$ ($S = 0$), respectively. As evidenced by EPR spectroscopy, the unpaired electron in the neutral species resides in a metal-centered a_1 (d_{z^2}) orbital.

dx.doi.org/10.1021/ic302799s | Inorg. Chem. 2013, 52, 2242−2256

CONCLUSION

We have shown experimentally (in part) and by DFT calculations that the electronic structures of tris(bipyridine) complexes of the early transition metal ions may be described as follows.

Monocation $[Ti(bpy)_3]^{1+}$ ($S = {}^1/_2$). This complex is best formulated as $[Ti^{III}(bpy^{\bullet})_2(bpy^0)]^{1+}$, with the $S = {}^1/_2$ ground state resulting from a strong intramolecular antiferromagnetic coupling between the central Ti^{III} ion (d^1) and one of the $(bpy^{\bullet})^{1-}$ ligands. Hence, the unpaired spin is ligand-centered.

Neutral $[M(bpy)_3]^0$ Species (M = Sc, Y, Ti, Zr, Hf, V, Nb, Ta). $[Sc^{III}(bpy^{\bullet})_3]^0$ and $[Y^{III}(bpy^{\bullet})_3]^0$ both contain d^0 metal ions and three $(bpy^{\bullet})^{1-}$ ligands, plus spin-frustrated ligand-centered $S = {}^1/_2$ ground states that derive from weak intramolecular ligand radical−radical antiferromagnetic coupling. The $S = {}^3/_2$ excited states are energetically low lying. The diamagnetic ($S = 0$) ground state of $[Ti^{III}(bpy^{\bullet})_3]^0$ is attained via intramolecular antiferromagnetic coupling of a central Ti^{III} ion (d^1) with a $(bpy^{\bullet})^{1-}$ ligand, plus antiferromagnetic coupling between the two remaining $(bpy^{\bullet})^{1-}$ radicals. Both $[M(bpy)_3]^0$, where M = Hf and Zr, contain a central d^0 metal ion and consequently a distorted trigonal prismatic MN_6 polyhedron. Hence, they are best described as $[Zr^{IV}(bpy^{\bullet})_2(bpy^{2-})]^0$ and $[Hf^{IV}(bpy^{\bullet})_2(bpy^{2-})]^0$, wherein the two $(bpy^{\bullet})^{1-}$ radicals strongly intramolecularly antiferromagnetically couple with one another to yield an $S = 0$ ground state. However, an alternative description of their electronic structures as $[M^{IV}(bpy^{2-})_2(bpy^0)]^0$ ($S = 0$), which is a resonance form of $[M^{IV}(bpy^{\bullet})_2(bpy^{2-})]^0$, is conceivable. Whereas the neutral complex of vanadium has been shown to contain a central V^{II} d^3 ion and formulated $[V^{II}(bpy^{\bullet})_2(bpy^0)]^0$,[21b] the corresponding second and third row analogues display an inherent preference for higher oxidation states. More specifically, though $[Nb^{IV}(bpy^{2-})_2(bpy^0)]^0$ and $[Ta^{V}(bpy^{2-})_2(bpy^{\bullet})]^0$ both contain two $(bpy^{2-})^{2-}$ ligands and an $S = {}^1/_2$ ground state, the unpaired electron in the former case is metal-centered (d^1 ion and a neutral (bpy^0) ligand) and ligand-centered in the latter (d^0 ion and a $(bpy^{\bullet})^{1-}$ π-radical anion).

Monoanionic $[M(bpy)_3]^{1-}$ Species (M = Y, Ti, Zr, Hf, V, Nb, Ta). The complex $[Y^{III}(bpy^{\bullet})_2(bpy^{2-})]^{1-}$ was calculated to have an $S = 0$ ground state derived from the antiferromagnetic coupling of two $(bpy^{\bullet})^{1-}$ radicals mediated by a Y^{III} ion. The metal center in $[Ti^{III}(bpy^{\bullet})_2(bpy^{2-})]^{1-}$ can also be described as having a +III oxidation state, but strong antiferromagnetic coupling between the d^1 ion and the $(bpy^{\bullet})^{1-}$ ligand leaves an unpaired spin on the second $(bpy^{\bullet})^{1-}$ and creates an $S = {}^1/_2$ ground state. Once again, the Zr and Hf analogues contain the higher +IV oxidation state and are formulated $[Zr^{IV}(bpy^{2-})_2(bpy^{\bullet})]^{1-}$ and $[Hf^{IV}(bpy^{2-})_2(bpy^{\bullet})]^{1-}$ with ligand-centered doublet ground states. The diamagnetic Nb and Ta monoanions possess the electronic structures $[Nb^{IV}(bpy^{2-})(bpy^{\bullet})_2]^{1-}$ and $[Ta^{V}(bpy^{2-})_2]^{1-}$ (the $S = 0$ ground state in the former case is attained by intramolecular antiferromagnetic coupling of the d^1 metal ion and $(bpy^{\bullet})^{1-}$ ligand), whereas $[V^{II}(bpy^{\bullet})_3]^{1-}$ is most appropriate for their first row congener.[21b]

Dianionic $[M(bpy)_3]^{2-}$ Species (M = Y, Ti, Zr, Hf). The oxidation states of the central metal ions in these complexes remain the same as in their monoanionic counterparts. The additional electron is always ligand-centered: $[Y^{III}(bpy^{2-})_2(bpy^{\bullet})]^{2-}$ ($S = {}^1/_2$); $[Ti^{III}(bpy^{2-})_2(bpy^{\bullet})]^{1-}$ ($S = 0$); $[Zr^{IV}(bpy^{2-})_3]^{2-}$ ($S = 0$); $[Hf^{IV}(bpy^{2-})_3]^{2-}$ ($S = 0$). Interestingly, $[V^{II}(bpy^{\bullet})_2(bpy^{2-})]^{2-}$ has proved to be experimentally inaccessible.

Trianionic $[M(bpy)_3]^{3-}$ Species (M = Y, Ti). $[Y^{III}(bpy^{2-})_3]^{3-}$ ($S = 0$) and $[Ti^{III}(bpy^{2-})_3]^{3-}$ ($S = {}^1/_2$) both contain fully reduced ligand dianions $(bpy^{2-})^{2-}$ and trivalent d^0 and d^1 metal ions, respectively.

The most striking and remarkable feature of all the series of complexes investigated herein is that all redox events are largely ligand-centered. In other words, the oxidation states of the individual metals (i.e., Sc^{III}, Y^{III}, Ti^{III}, Zr^{IV}, Hf^{IV}, V^{II}, Nb^{IV}, Ta^{V}) are retained throughout.

ASSOCIATED CONTENT

Supporting Information

Crystallographic information files (CIF) for $[Na(THF)_5][Ta(^tbpy)_3]$ and further information regarding the DFT calculations, including tables of atomic coordinates, bond distances, and energies, plus additional Mulliken spin density plots and qualitative frontier molecular orbital diagrams. This material is available free of charge via the Internet at http://pubs.acs.org.

AUTHOR INFORMATION

Corresponding Author

*E-mail: karl.wieghardt@cec.mpg.de.

Present Address

[§]Brown Science Center, Department of Chemistry, Transylvania University, 300 North Broadway, Lexington, KY 40508, United States.

Notes

The authors declare no competing financial interest.

ACKNOWLEDGMENTS

We thank the Max Planck Society for financial support, and Ms. Heike Schucht and Mr. Andreas Göbels for technical assistance. Portions of this research were carried out at the Stanford Synchrotron Radiation Lightsource, a Directorate of SLAC National Accelerator Laboratory and an Office of Science User Facility operated by the U.S. Department of Energy Office of Science by Stanford University. The SSRL Structural Molecular Biology Program is supported by the DOE Office of Biological and Environmental Research, and by the National Institutes of Health, National Center for Research Resources, Biomedical Technology Program.

REFERENCES

(1) Early reviews: (a) Constable, E. C. *Adv. Inorg. Chem.* **1989**, *34*, 1−37. (b) Kaim, W. *Chem. Ber.* **1981**, *114*, 3789.

(2) In this Article, we use the abbreviations bpy and ^{t}bpy in a generic sense; i.e., in these cases we do not wish to assign a specific oxidation level of these ligands. In contrast, we use bpy^0 to indicate the presence of a diamagnetic neutral ligand ($S_L = 0$), $(bpy^{\bullet})^{1-}$ for the π radical monoanion ($S_L = {}^1/_2$), and $(bpy^{2-})^{2-}$ for the diamagnetic dianion ($S_L = 0$).

(3) (a) Crawford, N. P.; Melson, G. A. *Inorg. Nucl. Chem. Lett.* **1968**, *4*, 399. (b) Crawford, N. P.; Melson, G. A. *J. Chem. Soc., A* **1969**, 427.

(4) (a) Herzog, S.; Byhan, G.; Wulfert, P. *Z. Chem.* **1961**, *1*, 370. (b) Inove, M.; Horiba, T.; Hara, K. *Bull. Chem. Soc. Jpn.* **1978**, *51*, 3073.

(5) Herzog, S.; Gustav, K. *Z. Naturforsch.* **1962**, *17b*, 62.

(6) Herzog, S.; Grimm, U. *Z. Chem.* **1967**, *7*, 432.

(7) Nikiforov, G. B.; Roesky, H. W.; Noltemeyer, M.; Schmidt, H.-G. *Polyhedron* **2004**, *23*, 561.

(8) (a) Synthesis: Herzog, S.; Taube, R. *Z. Anorg. Allg. Chem.* **1960**, *306*, 159. (b) UV-vis spectra: Pappalardo, R. *Inorg. Chim. Acta* **1968**,

2, 209. (c) König, E.; Herzog, S. *J. Inorg. Nucl. Chem.* **1970**, *32*, 613. (d) Intrared spectrum: König, E.; Lindner, E. *Spectrochim. Acta* **1972**, *28A*, 1393. (e) EPR spectrum: König, E. *Z. Naturforsch.* **1964**, *19a*, 1139. (f) X-ray structure: Albrecht, G. *Z. Chem.* **1963**, *3*, 182. (g) UV−vis spectra: Hanazaki, I.; Nagakura, S. *Bull. Chem. Soc. Jpn.* **1971**, *44*, 2312. (h) Kaizu, Y.; Yazaki, T.; Torii, Y.; Kobayashi, H. *Bull. Chem. Soc. Jpn.* **1970**, *43*, 2068. (i) ^{1}H NMR: Flamini, A.; Giuliani, A. M. *Inorg. Chim. Acta* **1986**, *112*, L7.

(9) Herzog, S.; Gutsche, E. *Z. Chem.* **1963**, *3*, 393.

(10) Herzog, S.; Zühlke, M. *Z. Chem.* **1966**, *6*, 434.

(11) Herzog, S.; Grimm, U. *Z. Chem.* **1968**, *8*, 186.

(12) Herzog, S.; Zühlke, H. *Z. Naturforsch.* **1960**, *15b*, 466.

(13) Quirk, J.; Wilkinson, G. *Polyhedron* **1982**, *1*, 209.

(14) Herzog, S.; Zühlke, H. *Z. Chem.* **1966**, *6*, 382.

(15) Rosa, P.; Mézailles, N.; Ricard, L.; Mathey, F.; LeFloch, P. *Angew. Chem., Int. Ed.* **2000**, *39*, 1823.

(16) Herzog, S.; Schuster, R. *Z. Naturforsch.* **1962**, *17b*, 62.

(17) Herzog, S.; Wulf, E. *Z. Chem.* **1966**, *6*, 434.

(18) Bellavance, P.; Corey, E. J.; Corey, J. Y.; Hey, G. *Inorg. Chem.* **1977**, *16*, 462.

(19) (a) Irwin, M.; Jenkins, R. K.; Denning, M. S.; Krämer, T.; Grandjean, F.; Long, G. J.; Merchel, R.; McGrady, J. E.; Goicoechea, J. M. *Inorg. Chem.* **2010**, *49*, 6160. (b) Irwin, M.; Doyle, L. R.; Krämer, T.; Herchel, R.; McGrady, J. E.; Goicoechea, J. M. *Inorg. Chem.* **2012**, *51*, 12301. (c) Gore-Randall, E.; Irwin, M.; Denning, M. S.; Goicoechea, J. M. *Inorg. Chem.* **2009**, *48*, 8304.

(20) Roitershtein, D.; Domingos, A.; Pereira, L. C. J.; Ascenso, J. R.; Marques, N. *Inorg. Chem.* **2003**, *42*, 7666.

(21) (a) Scarborough, C. C.; Sproules, S.; Weyhermüller, T.; DeBeer, S.; Wieghardt, K. *Inorg. Chem.* **2011**, *50*, 12446. (b) Bowman, A. C.; Sproules, S.; Wieghardt, K. *Inorg. Chem.* **2012**, *51*, 3707. (c) England, J.; Scarborough, C. C.; Weyhermüller, T.; Sproules, S.; Wieghardt, K. *Eur. J. Inorg. Chem.* **2012**, 4605.

(22) Hanson, G. R.; Gates, K. E.; Noble, C. J.; Griffin, M.; Mitchell, A.; Benson, S. *J. Inorg. Biochem.* **2004**, *98*, 903.

(23) George, G. N. *EXAFSPAK & EDG_FIT*; Stanford Synchrotron Radiation Lightsource, Stanford Linear Accelerator Center, Stanford University: Palo Alto, CA, 2000.

(24) Neese, F. *Orca, an Ab Initio Density Functional and Semiempirical Electronic Structure Program Package*, version 2.8, revision 2287; Universität Bonn: Bonn, Germany, 2010.

(25) (a) Becke, A. D. *Phys. Rev. A* **1988**, *38*, 3098. (b) Becke, A. D. *J. Chem. Phys.* **1993**, *98*, 5648. (c) Lee, C. T.; Yang, W. T.; Parr, R. G. *Phys. Rev. B* **1988**, *37*, 785.

(26) (a) Weigend, F.; Ahlrichs, R. *Phys. Chem. Chem. Phys.* **2005**, *7*, 3297. (b) Schäfer, A.; Huber, C.; Ahlrichs, R. *J. Chem. Phys.* **1994**, *100*, 5829.

(27) (a) Schäfer, A.; Horn, H.; Ahlrichs, R. *J. Chem. Phys.* **1992**, *97*, 2571.

(28) (a) van Wuellen, C. *J. Chem. Phys.* **1998**, *109*, 392. (b) van Leuthe, E.; Baerends, E. J.; Snijders, J. G. *J. Chem. Phys.* **1993**, *99*, 4597. (c) van Lenthe, E.; Baerends, E. J.; Snijders, J. G. *J. Chem. Phys.* **1994**, *101*, 9783. (d) Pantazis, D. A.; Chen, X. Y.; Landis, C. R.; Neese, F. *J. Chem. Theory Comput.* **2008**, *4*, 908.

(29) (a) Eichkorn, K.; Weigend, F.; Treutler, O.; Ahlrichs, R. *Theor. Chem. Acc.* **1997**, *97*, 119. (b) Eichkorn, K.; Treutler, O.; Öhm, H.; Häser, M.; Ahlrichs, R. *Chem. Phys. Lett.* **1995**, *240*, 283. (c) Eichkorn, K.; Treutler, O.; Öhm, H.; Häser, M.; Ahlrichs, R. *Chem. Phys. Lett.* **1995**, *242*, 652.

(30) (a) Neese, F.; Wennmohs, F.; Hansen, A.; Becker, U. *Chem. Phys.* **2009**, *356*, 98. (b) Kossmann, S.; Neese, F. *Chem. Phys. Lett.* **2009**, *481*, 240. (c) Neese, F. *J. Comput. Chem.* **2003**, *24*, 1714.

(31) Klamt, A.; Schüürmann, G. *J. Chem. Soc., Perkin Trans. 2* **1993**, 799.

(32) (a) Grimme, S. *J. Comput. Chem.* **2004**, *25*, 1463. (b) Grimme, S. *J. Comput. Chem.* **2006**, *27*, 1787. (c) Grimme, S.; Antony, J.; Ehrlich, S.; Krieg, H. *J. Chem. Phys.* **2010**, *132*, 154104.

(33) (a) Pulay, P. *Chem. Phys. Lett.* **1980**, *73*, 393. (b) Pulay, P. *J. Comput. Chem.* **1992**, *3*, 556.

(34) (a) Noodleman, L. *J. Chem. Phys.* **1981**, *74*, 5737. (b) Noodleman, L.; Norman, J. G.; Osborne, J. H.; Aizman, A.; Case, D. A. *J. Am. Chem. Soc.* **1985**, *107*, 3418. (c) Noodleman, L.; Davidson, E. R. *Chem. Phys.* **1986**, *109*, 131. (d) Noodleman, L.; Case, D. A.; Aizman, A. *J. Am. Chem. Soc.* **1988**, *110*, 1001. (e) Noodleman, L.; Peng, C. Y.; Case, D. A.; Monesca, J. M. *Coord. Chem. Rev.* **1995**, *144*, 199. (f) Soda, T.; Kitagawa, Y.; Onishi, T.; Takano, Y.; Shigetu, Y.; Nagao, H.; Yoshioka, Y.; Yamaguchi, K. *Chem. Phys. Lett.* **2000**, *319*, 223. (g) Yamaguchi, K.; Takahara, Y.; Fueno, T. In *Applied Quantum Chemistry*; Smith, V. H., Ed.; Reidel: Dordecht, The Netherlands, 1986; p 155.

(35) Neese, F. *J. Phys. Chem. Solids* **2004**, *65*, 781.

(36) Pettersen, E. F.; Goddard, T. D.; Huang, C. C.; Couch, G. S.; Greenblatt, D. M.; Meng, E. C.; Ferrin, T. E. *J. Comput. Chem.* **2004**, *25*, 1605.

(37) (a) Sheldrick, G. M. *SADABS, Bruker-Siemens Area Detector Absorption and Other Corrections, Version 2008/1*; University of Göttingen: Göttingen, Germany, 2006. (b) *ShelXTL 6.14*; Bruker AXS Inc.: Madison, WI, 2003. (c) Sheldrick, G. M. *ShelXL97*; University of Göttingen: Göttingen, Germany, 1997.

(38) König, E.; Kremer, S. *Chem. Phys. Lett.* **1970**, *5*, 87.

(39) (a) Heath, G. A.; Yellowlees, L. J.; Braterman, P. S. *J. Chem. Soc., Chem. Commun.* **1981**, 287. (b) Heath, G. A.; Yellowlees, L. J.; Braterman, P. S. *Chem. Phys. Lett.* **1982**, *92*, 646.

(40) Carrington, A.; McLachlan, A. D. *Introduction to Magnetic Resonance*; Harper & Row: New York, 1967.

(41) (a) Spikes, G. H.; Sproules, S.; Bill, E.; Weyhermüller, T.; Wieghardt, K. *Inorg. Chem.* **2008**, *47*, 10935. (b) Sproules, S.; Weyhermüller, T.; DeBeer, S.; Wieghardt, K. *Inorg. Chem.* **2010**, *49*, 5241.

(42) Wong, E. W.; Walsby, C. J.; Storr, T.; Leznoff, D. B. *Inorg. Chem.* **2010**, *49*, 3343.

(43) Shulman, R. G.; Yafet, Y.; Eisenberger, P.; Blumberg, W. E. *Proc. Natl. Acad. Sci. U.S.A.* **1976**, *73*, 1384.

(44) Sproules, S.; Benedito, F. L.; Bill, E.; Weyhermüller, T.; DeBeer George, S.; Wieghardt, K. *Inorg. Chem.* **2009**, *48*, 10926.

(45) Bock, H.; Lehn, J.-M.; Pauls, J.; Holl, S.; Krenzel, V. *Angew. Chem., Int. Ed.* **1999**, *38*, 952.

(46) Buttery, J. H. N.; Effendy; Mutrofin, S.; Plackett, N. C.; Skelton, B. W.; Whitaker, C. R.; White, A. H. *Z. Anorg. Allg. Chem.* **2006**, *632*, 1851.

(47) Scarborough, C. C.; Wieghardt, K. *Inorg. Chem.* **2011**, *50*, 9773.

(48) Nikiforov, G. B.; Roesky, H. W.; Noltemeyer, M.; Schmidt, H.-G. *Polyhedron* **2004**, *23*, 561.

(49) Rosa, P.; Mézailles, N.; Ricard, L.; Mathey, F.; LeFloch, P. *Angew. Chem., Int. Ed.* **2000**, *39*, 1823.

(50) Wulf, E.; Herzog, S. *Z. Anorg. Allg. Chem.* **1972**, *387*, 81.

(51) Inoue, M.; Horiba, T.; Hara, K. *Bull. Chem. Soc. Jpn.* **1978**, *51*, 3073.

(52) Scarborough, C. C.; Lancaster, K. M.; DeBeer, S.; Weyhermüller, T.; Sproules, S.; Wieghardt, K. *Inorg. Chem.* **2012**, *51*, 3718.

(53) Kahn, O. *Molecular Magnetism*; Wiley-VCH Inc.: New York, 1993.

(54) Herzog, S.; Gustav, K. *Z. Anorg. Allg. Chem.* **1966**, *346*, 150.

(55) Daff, P. J.; Etienne, M.; Donnadieu, B.; Knottenbelt, S. Z.; McGrady, J. E. *J. Am. Chem. Soc.* **2002**, *124*, 3818.